Article

Molecular Cell

N^6-Methyladenosine Guides mRNA Alternative Translation during Integrated Stress Response

Graphical Abstract

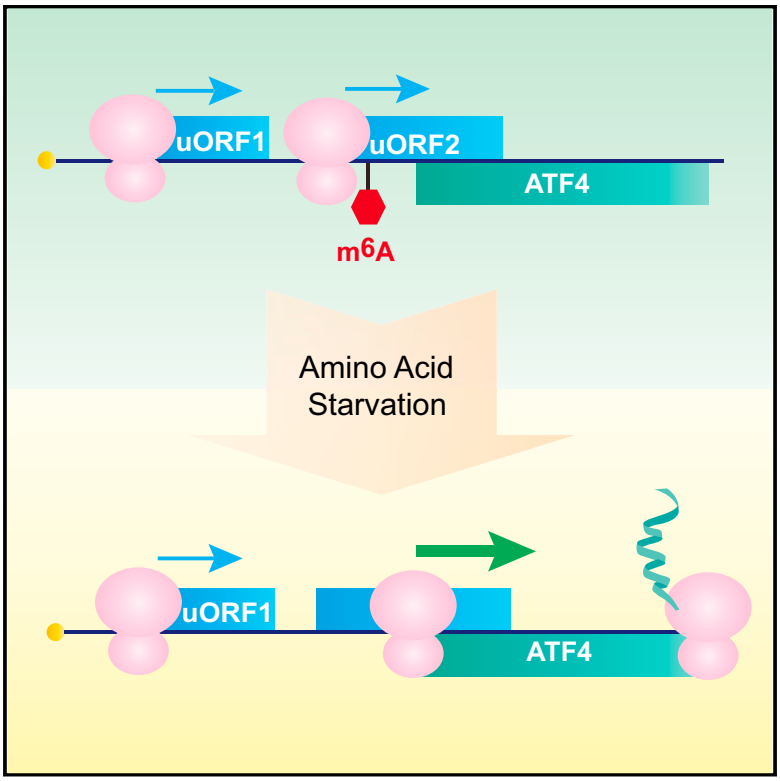

Authors

Jun Zhou, Ji Wan, Xin Erica Shu, ..., Martin E. Hess, Jens C. Brüning, Shu-Bing Qian

Correspondence

sq38@cornell.edu

In Brief

Zhou et al. show that amino acid starvation-induced ATF4 translation is subject to regulation by mRNA methylation in the form of m^6A. Global analysis of translation initiation reveals that m^6A in the 5′ UTR modulates start codon selection, thereby controlling alternative translation.

Highlights

- ATF4 reinitiation involves the m^6A demethylase ALKBH5
- ATF4 reinitiation is sensitive to mRNA m^6A levels
- Global alternative translation is modulated by 5′ UTR m^6A levels
- Liver-specific FTO transgenic mice show altered translation initiation

Zhou et al., 2018, Molecular Cell 69, 636–647
February 15, 2018
https://doi.org/10.1016/j.molcel.2018.01.019

CellPress

CellPress

Molecular Cell
Article

N^6-Methyladenosine Guides mRNA Alternative Translation during Integrated Stress Response

Jun Zhou,[1] Ji Wan,[1] Xin Erica Shu,[1] Yuanhui Mao,[1] Xiao-Min Liu,[1] Xin Yuan,[1] Xingqian Zhang,[1] Martin E. Hess,[2] Jens C. Brüning,[2] and Shu-Bing Qian[1,3,*]

[1]Division of Nutritional Sciences, Cornell University, Ithaca, NY 14853, USA
[2]Max Planck Institute for Metabolism Research, Cologne 50931, Germany
[3]Lead Contact
*Correspondence: sq38@cornell.edu
https://doi.org/10.1016/j.molcel.2018.01.019

SUMMARY

The integrated stress response (ISR) facilitates cellular adaptation to stress conditions via the common target eIF2α. During ISR, the selective translation of stress-related mRNAs often relies on alternative mechanisms, such as leaky scanning or reinitiation, but the underlying mechanism remains incompletely understood. Here we report that, in response to amino acid starvation, the reinitiation of ATF4 is not only governed by the eIF2α signaling pathway, but is also subjected to regulation by mRNA methylation in the form of N^6-methyladenosine (m^6A). While depleting m^6A demethylases represses ATF4 reinitiation, knocking down m^6A methyltransferases promotes ATF4 translation. We demonstrate that m^6A in the 5′ UTR controls ribosome scanning and subsequent start codon selection. Global profiling of initiating ribosomes reveals widespread alternative translation events influenced by dynamic mRNA methylation. Consistently, *Fto* transgenic mice manifest enhanced ATF4 expression, highlighting the critical role of m^6A in translational regulation of ISR at cellular and organismal levels.

INTRODUCTION

Eukaryotic cells employ a cap-dependent scanning mechanism to initiate translation for most mRNAs (Gebauer and Hentze, 2004; Jackson et al., 2010; Sonenberg and Hinnebusch, 2009). Following recognition of the m^7G cap structure, the assembled 43S pre-initiation complex (PIC) searches for the first AUG start codon in a favorable sequence context by scanning the message from the 5′ end (Hinnebusch, 2014). When the context of the upstream AUG triplet is not optimal, a subpopulation of 43S complexes continue to scan and initiate at a downstream site, in a process known as leaky scanning. If the selected upstream AUG is followed by a short upstream open reading frame (uORF), a significant fraction of ribosomes resume scanning after termination, resulting in reinitiation at downstream start codons. Both leaky scanning and reinitiation events contribute to alternative translation, which facilitates cellular adaptation to a variety of stress conditions (Liu and Qian, 2014; Sonenberg and Hinnebusch, 2007). The integrated stress response (ISR) is characterized by regulated alternative translation of uORFs in response to phosphorylation of the α subunit of eukaryotic initiation factor 2 (eIF2α) (Harding et al., 2002; Wek et al., 2006). Phosphorylation of eIF2α converts eIF2-GDP into a competitive inhibitor of the guanine nucleotide exchange factor eIF2B and thereby reduces eIF2-GTP-$tRNA_i^{Met}$ ternary complex (TC) formation. As a result, global translation is severely attenuated. However, a cadre of stress-related mRNAs undergo sustained or even upregulated translation. Many of these messages harbor multiple uORFs. Despite the prevailing view that TC availability controls the efficiency of uORF translation, whether additional mechanisms exist to influence alternative translation remains poorly understood.

N^6-methyladenosine (m^6A) is the most common internal modification in eukaryotic mRNA (Fu et al., 2014; Meyer and Jaffrey, 2014). Recognizing the core consensus sequence RRACH (R, purine; H, non-guanine base), the responsible methyltransferase has been identified as a functional complex consisting of METTL3, METTL14, and WTAP (Bokar et al., 1997; Liu et al., 2014; Ping et al., 2014). The discovery of FTO and ALKBH5 in the demethylation pathway suggests that m^6A modification is reversible (Jia et al., 2011; Zheng et al., 2013). Serving as an epitranscriptomic layer of gene regulation, dynamic m^6A modification has been implicated in a wide range of RNA metabolism including mRNA stability (Wang et al., 2014), splicing (Xiao et al., 2016), microRNA processing (Alarcón et al., 2015), RNA secondary structure (Liu et al., 2015), and translation (Meyer et al., 2015; Wang et al., 2015; Zhou et al., 2015). The transcriptome-wide m^6A mapping revealed asymmetric distribution of mRNA methylation with the majority of m^6A sites enriched near the stop codon (Dominissini et al., 2012; Meyer et al., 2012). However, m^6A also occurs in the coding region (CDS) as well as 5′ UTR. Crucial for ribosome recruitment to mRNA, 5′ UTR contains many regulatory elements that determine the initiation mode and start codon selection (Hinnebusch et al., 2016). We recently reported that 5′ UTR methylation in the form of m^6A enables cap-independent translation (Meyer et al., 2015; Zhou et al., 2015). However, it remains to be addressed whether and how mRNA methylation in the 5′ UTR influences alternative translation.

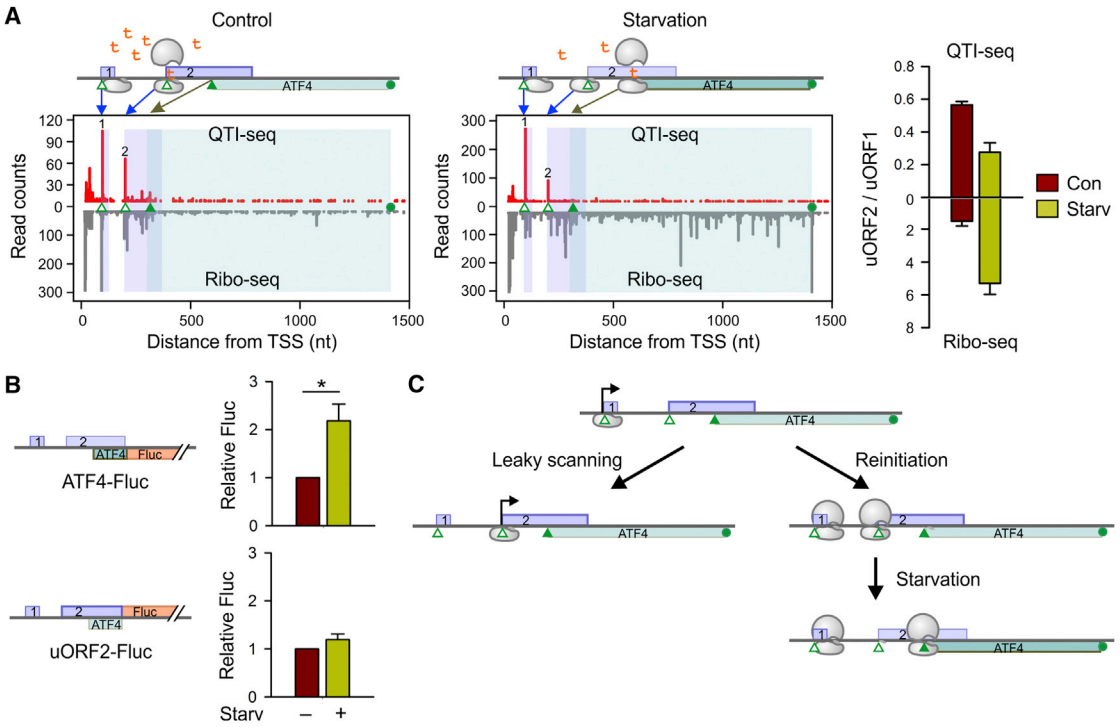

Figure 1. Starvation-Induced ATF4 Reinitiation with Sustained uORF2 Translation

(A) A delayed reinitiation model is shown for ATF4 translation in response to amino acid starvation (top panels). MEF cells with or without amino acid starvation were subject to QTI-seq and Ribo-seq. Reads mapped to *Atf4* are presented in bar graphs. Green triangles denote TIS codons with the solid triangle as the aTIS. Right panel shows the quantification of uORF2 translation. Both Ribo-seq and QTI-seq reads mapped to uORF2 are normalized to uORF1. Error bars, mean ± SEM; n = 3 biological replicates.

(B) Illustration of ATF-Fluc and uORF2-Fluc reporters. MEF cells transfected with reporter plasmids were subjected to amino acid starvation for 6 hr, followed by luminometry. Fluc activities are normalized to Rluc. Error bars, mean ± SEM; *p < 0.05, n = 3 biological replicates.

(C) Schematic of uORF2 translation via leaky scanning (left panel) or reinitiation (right panel). Migrating 80S ribosomes are inaccessible to LTM binding, resulting in the failure of QTI-seq to capture initiating ribosomes during ATF4 reinitiation.

See also Figure S1.

Here we set out to investigate the role of 5′ UTR methylation in translational regulation of ISR. Among ISR-induced alternative translation events, the best characterized example is GCN4 in yeast or ATF4 in mammals (Dever et al., 1992; Mueller and Hinnebusch, 1986). Using cell culture and transgenic mouse models, we found that differential mRNA methylation readily influences ATF4 translation in response to amino acid starvation. By coupling m^6A sequencing (m^6A-seq) with quantitative profiling of initiating ribosomes, we uncovered a critical role for 5′ UTR methylation in ribosome scanning and alternative start codon selection. This finding not only adds a new dimension to translational regulation of ISR, but also expands the functional diversity of mRNA methylation in fundamental cellular processes.

RESULTS

Translational Regulation of ATF4

The mature transcript of *ATF4* contains two uORFs in the 5′ UTR: one near the 5′ terminus and the other overlapping with the CDS but in different reading frames (Figure 1A, top panel). The short uORF1 permits reinitiation when the recycled ribosome remains on the message together with some of the original initiation factors. Unlike leaky scanning in which the 43S PIC already contains a TC, the reinitiating ribosome needs to acquire a new TC before selecting the downstream start codon. Under the normal growth condition with abundant TC levels, reinitiation readily occurs at the start codon of uORF2, thereby suppressing ATF4 translation. During ISR, with limited TC availability as a result of eIF2α phosphorylation, the migrating ribosome scans through uORF2 and becomes available to initiate translation of the downstream CDS (Vattem and Wek, 2004). The delayed reinitiation model predicts that the upregulation of ATF4 synthesis is a direct result of reduced uORF2 translation. To experimentally demonstrate this feature, we applied quantitative translation initiation sequencing (QTI-seq) to a mouse embryonic fibroblast (MEF) cell line with or without amino acid starvation. QTI-seq permits global mapping of translation initiation sites (TISs) and quantitative measurement of the ribosome density at individual TISs (Gao et al., 2015). Under the nutrient-rich condition, QTI-seq revealed clear TIS peaks of uORF1 and uORF2, but not the main CDS of ATF4 (Figure 1A). As expected, Ribo-seq showed only background levels of ribosome density across the main CDS, while displaying a considerable amount of footprints in uORF2. Upon

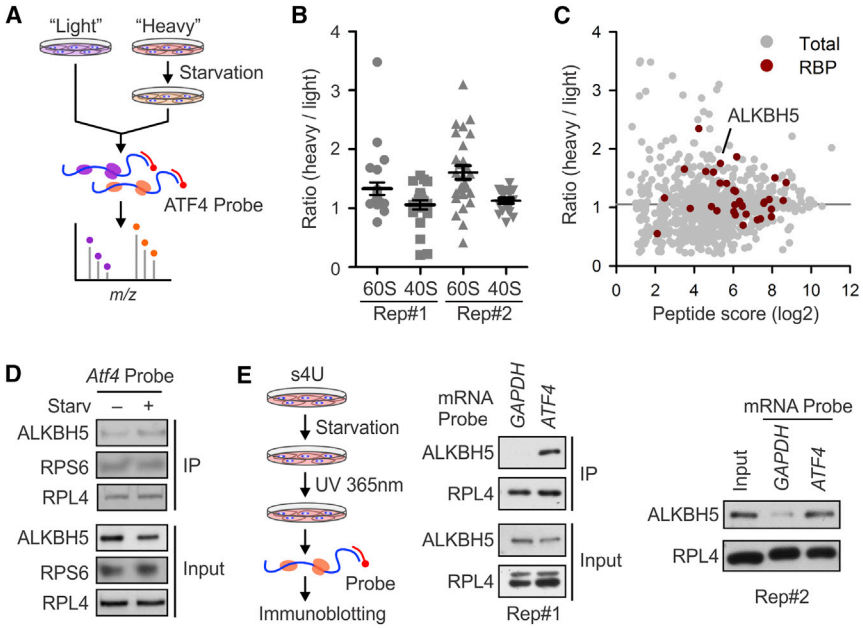

Figure 2. Quantitative Proteomics of ATF4 Translation

(A) Schematic of SILAC. MEF cells were cultured in "light" or "heavy" media for five passages before treating "heavy" cells with amino acid starvation for 2 hr. *Atf4* mRNA and associated proteins were purified by a biotinylated probe followed by mass spectrometry.

(B) Relative ratio of *Atf4* mRNA-associated 60S and 40S ribosomal proteins before and after amino acid starvation. Two biological replicates are shown.

(C) A scatterplot shows *Atf4* mRNA-associated proteins before and after amino acid starvation. The original peptide score (log_2) and starvation-induced fold changes are shown in the x axis and the y axis, respectively. RNA-binding proteins (RBPs) are highlighted with ALKBH5 indicated.

(D) Validation of *Atf4* mRNA-associated ALKBH5 by immunoblotting using the same sample as in (C).

(E) Schematic of zero-distance crosslinking methodology. 4-Thiouridine (s^4U)-labeled RNAs were crosslinked to directly associated proteins using 365 nm UV. *Gapdh* or *Atf4* mRNAs were purified by biotinylated probes followed by immunoblotting.

See also Figure S2.

amino acid starvation, a large amount of footprints appeared in the main CDS, which is consistent with the increased translation of ATF4 (Figure 1A, right panel). Surprisingly, uORF2 also showed an increased read density, but the upstream TIS (uTIS) peak associated with uORF2 was reduced. The unexpected discordance between the TIS density and the CDS occupancy is also observable in HEK293 cells (Figure S1A).

Since uORF2 overlaps with the main CDS, the increased uORF2 read density upon starvation could be overestimated. To directly examine the translational status of overlapping ORFs in cells with or without amino acid deprivation, we constructed firefly luciferase (Fluc) reporters by replacing the main CDS of ATF4 with Fluc or fusing Fluc to the uORF2 (Figure 1B). Similar to the endogenous ATF4, amino acid starvation triggered translation of ATF4-Fluc. However, translation of uORF2-Fluc did not show any corresponding decrease in these starved cells. A recent study using T cells recognizing tracing peptides also reported sustained uORF2 translation in the absence or presence of ISR (Starck et al., 2016). Therefore, starvation-induced ATF4 synthesis does not seem to be a direct consequence of reduced uORF2 translation.

Interestingly, QTI-seq failed to capture the initiating ribosome at the start codon of the main CDS even after starvation (Figure 1A). QTI-seq relies on direct binding of lactimidomycin (LTM) to an empty E-site formed during 60S joining, but not 80S (Lee et al., 2012). It is possible that ATF4 reinitiation involves post-termination 80S ribosomes migrated from uORF1 (Figure 1C). Supporting this notion, previous studies using a reconstituted *in vitro* system demonstrated that some reinitiation events involve 80S ribosomes rather than 40S subunits (Skabkin et al., 2013). In the case of ATF4, 80S footprints were indeed discernable between uORF1 and uORF2. To generalize this finding, we selected transcripts bearing non-overlapping uORFs. Interestingly, the read density within the "inter" region of uORFs is significantly higher than 5′ UTR ($p < 2.2E{-}16$; Figure S1B). To exclude the possibility that the "inter" read density is a result of stop codon read through from uORF1, we analyzed the phasing property of 80S reads found in the "inter" region of uORFs. While uORF1 and uORF2 showed a strong 3-nt periodicity, virtually no periodicity was found for the "inter" reads (Figure S1C). It is likely that the reinitiation of ATF4 relies on mechanisms more complex than previously thought.

ATF4 Reinitiation Involves 80S Ribosomes and ALKBH5

To probe the mode of ATF4 reinitiation *in vivo*, we attempted to measure the relative ratio of ribosome subunits bound to *ATF4* mRNA before and after amino acid starvation. We reasoned that, if ATF4 reinitiation requires recycled 40S, more 40S subunits relative to 60S should become associated with *ATF4* mRNA upon starvation. We employed quantitative proteomics using stable isotope labeling by amino acids in cell culture (SILAC) (Figure 2A). Differentially labeled MEF cells were subjected to starvation ("heavy") or not ("light") followed by *ATF4* mRNA purification using a biotinylated probe. From two biological replicates, the 40S subunits constantly showed a relatively lower recovery than 60S from *ATF4* mRNA in response to starvation (Figure 2B). Although the relative abundance of each ribosomal protein varies, the overall differences between 60S and 40S proteins are apparent. This result supports the possibility that ATF4 reinitiation involves post-terminating 80S ribosomes. The exact nature of 80S migration during ATF4 reinitiation, however, merits further investigation.

The SILAC datasets also revealed many RNA-binding proteins (RBPs) associated with *ATF4* mRNA (Figure 2C; Table S1). Unexpectedly, we observed a modest increase of ALKBH5 (1.6- and 1.88-fold from two biological replicates), a well-characterized m^6A demethylase for single-stranded RNA (Xu et al., 2014; Zheng et al., 2013). The *ATF4* mRNA-associated ALKBH5 was

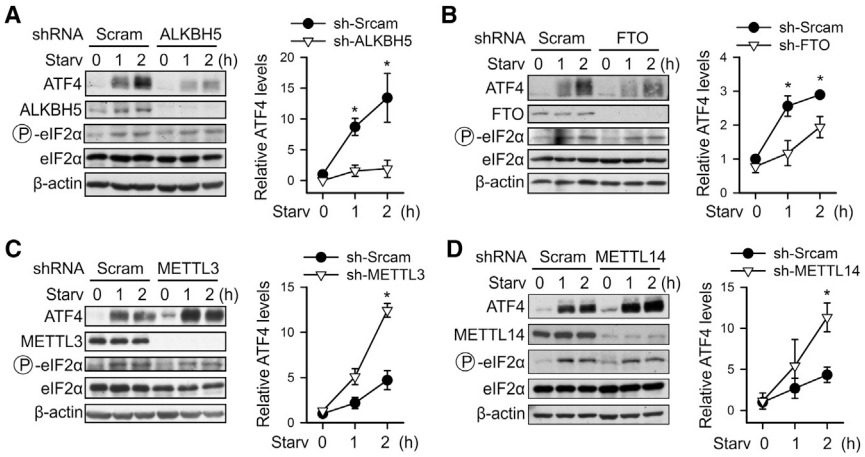

Figure 3. mRNA Methylation Influences ATF4 Translation

(A) MEF cells with or without ALKBH5 knockdown were subject to amino acid starvation followed by immunoblotting. The right panel shows the relative ATF4 levels quantified by densitometry and normalized to β-actin.

(B) MEF cells with or without FTO knockdown were subject to amino acid starvation followed by immunoblotting. The right panel shows the relative ATF4 levels quantified by densitometry and normalized to β-actin.

(C) MEF cells with or without METTL3 knockdown were subject to amino acid starvation followed by immunoblotting. The right panel shows the relative ATF4 levels quantified by densitometry and normalized to β-actin.

(D) MEF cells with or without METTL14 knockdown were subject to amino acid starvation followed by immunoblotting. The right panel shows the relative ATF4 levels quantified by densitometry and normalized to β-actin.

Error bars, mean ± SEM; n = 3 biological replicates. *$p < 0.05$.

confirmed using immunoblotting of the same sample (Figure 2D). It is unclear whether ALKBH5 binds directly to *ATF4* mRNA or indirectly via protein complex formation. To address this question, we applied zero-distance crosslinking of 4-thiouridine (s^4U)-labeled RNAs with endogenous proteins inside cells (Figure 2E). *ATF4* mRNA, but not *GAPDH*, readily pull down ALKBH5, although both messages were associated with a comparable amount of the ribosomal protein RPL4. This result suggests a potential role for mRNA m^6A modification in starvation-induced ATF4 translation.

Differential mRNA Methylation Influences ATF4 Translation

To investigate whether m^6A demethylases play a role in ATF4 translation, we used a lentiviral short hairpin RNA (shRNA) to knock down ALKBH5 from MEF cells. Upon amino acid starvation, ATF4 synthesis was significantly reduced in cells lacking ALKBH5 (Figure 3A). This was not due to the deficient eIF2α signaling pathway because ALKBH5 knockdown had little effect on the status of eIF2α phosphorylation. The comparable ATF4 mRNA levels in these cells strongly indicate that the reduced ATF4 expression occurred at the translational level (Figure S2A). Since FTO is another m^6A demethylase (Jia et al., 2011), we next examined whether FTO had the similar effect on ATF4 expression. Indeed, FTO depletion also dampened ATF4 expression following amino acid starvation (Figure 3B). Like ALKBH5 knockdown, silencing FTO affected neither the status of eIF2α phosphorylation nor ATF4 mRNA levels (Figure S2B). These results indicate a positive role for m^6A demethylases in ATF4 translation.

It is unclear whether it is the binding of demethylases per se or the subsequent changes of m^6A modification that influence ATF4 translation. To address this question, we used shRNA to silence METTL3, a core subunit of the methyltransferase complex (Liu et al., 2014). As expected, total mRNA methylation levels were reduced to about 50% in MEF cells lacking METTL3 as confirmed by m^6A blotting assay (Figure S2E). Remarkably, starvation-induced ATF4 translation was substantially enhanced in these cells (Figure 3C). As an independent validation, knocking down METTL14 also promoted ATF4 expression following amino acid starvation (Figure 3D). Once again, neither the eIF2α signaling pathway nor the steady-state levels of ATF4 mRNA were affected by silencing these methyltransferases in MEF cells (Figures S2C and S2D). Therefore, starvation-induced ATF4 translation is subjected to regulation by dynamic mRNA methylation in the form of m^6A.

uORF2 Methylation Controls Translation of ATF4

Dynamic m^6A modification has been implicated in translational regulation. Although 3′ UTR methylation seems to promote cap-dependent translation (Wang et al., 2015), 5′ UTR m^6A enables cap-independent translation (Meyer et al., 2015; Zhou et al., 2015). The ATF4 mRNA has a relatively short 3′ UTR and it is the 5′ UTR that bears regulatory uORFs. To probe the regional effects of mRNA methylation on ATF4 translation, we conducted m^6A-seq using RNAs purified from MEF cells with or without amino acid starvation. The message of ATF4 showed multiple m^6A peaks from 5′ UTR to CDS, but not in the 3′ UTR (Figure 4A). Interestingly, upon amino acid starvation, only the uORF2 region exhibited reduced m^6A levels. Notably, the peak located within uORF2 bears the m^6A consensus sequence GGAC. To affirm the site-specific methylation of uORF2, we devised site-specific m^6A detection by coupling m^6A antibody crosslinking with probe elongation (Figure S3). Quantitative m^6A printing revealed a nearly 3-fold reduction of methylation at ATF4 uORF2 (A225) upon amino acid starvation (Figure 4B; higher "probe+1" signals indicate lower methylation). The local change of m^6A in response to starvation is likely due to the substrate specificity of ALKBH5 or FTO that recognizes conformational markers signified by m^6A (Zou et al., 2016). Indeed, ALKBH5 only targets a small subset of m^6A sites installed by METTL3 as revealed by PAR-CLIP datasets (Figures S4A and S4B). In accordance with this notion, the uORF2 methylation

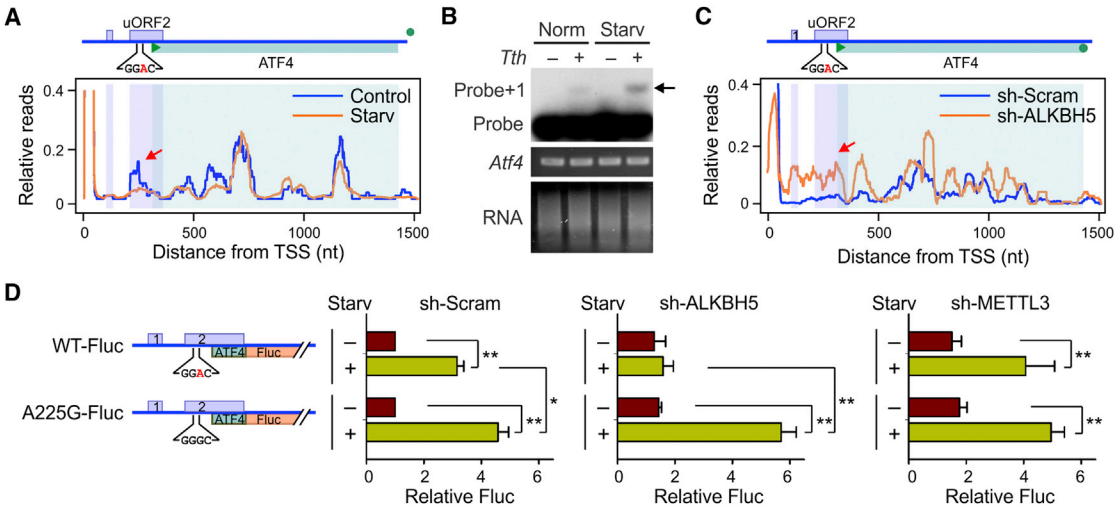

Figure 4. uORF2 Methylation Influences ATF4 Translation

(A) MEF cells with or without amino acid starvation were subject to m^{6}A-seq. Reads mapped to *Atf4* are presented in line graphs. *Atf4* uORF structure is shown above with m^{6}A consensus sequence highlighted. Red arrow indicates the corresponding m^{6}A peak.

(B) Site-specific detection of m^{6}A in *Atf4* uORF2. Autoradiography shows primer extended products of endogenous *Atf4* with or without amino acid starvation. Lower panel shows the *Atf4* input determined by semi-RT-PCR and the total mRNA stained by ethidium bromide.

(C) MEF cells with or without ALKBH5 knockdown were subject to m^{6}A-seq. Reads mapped to *Atf4* are presented in line graphs. *Atf4* uORF structure is shown above with m^{6}A consensus sequence highlighted. Red arrow indicates the corresponding m^{6}A peak.

(D) MEF cells with either ALKBH5 or METTL3 knockdown were transfected with reporter plasmids encoding ATF4-Fluc or ATF4(A225G)-Fluc. After amino acid starvation for 6 hr, Fluc activities were measured by luminometry. Error bars, mean ± SEM; n = 3 biological replicates. *p < 0.05; **p < 0.01.

See also Figures S3 and S4.

was restored in cells lacking either ALKBH5 or FTO (Figures 4C and S4C).

To resolve the putative role of uORF2 methylation in ATF4 translation, we introduced an A225G mutation into the Fluc reporter to prevent m^{6}A modification at this particular site. Compared to the wild-type control, the A225G mutant exhibited higher Fluc levels in response to starvation (Figure 4D), which is consistent with the negative role of uORF2 methylation in ATF4 translation. In cells with ALKBH5 knockdown, the wild-type reporter showed no response to starvation, which mimics the behavior of endogenous ATF4 (Figure 3A). Remarkably, the A225G mutant maintained a robust sensitivity to nutrient withdrawal by showing elevated Fluc levels (>5-fold). This result echoes the finding that lack of uORF2 methylation promotes translation of the downstream ATF4 main CDS. Further supporting this notion, in cells with METTL3 knockdown, both wild-type and mutant reporters exhibited high sensitivity to starvation and the difference in Fluc levels was virtually diminished (Figure 4D, right panel). The persistent Fluc expression from the A225G reporter was also seen in cells lacking FTO or METTL14 (Figure S4D). In addition, we observed similar behavior for Fluc reporters harboring A225C or A225U mutation (Figure S4D), excluding the possible codon-associated effects. Collectively, these results established the regulatory role of uORF2 methylation in translational control of ATF4 during ISR.

5′ UTR Methylation Controls Start Codon Selection

How does uORF2 methylation regulate the translation of the uORF2 itself as well as the main coding region of ATF4? m^{6}A modification could exert two opposing effects toward uORF2 translation: (1) m^{6}A sits within uORF2 and might act as a road block to elongating ribosomes. Indeed, m^{6}A in the coding region has been shown to slow down the decoding process (Choi et al., 2016). (2) uORF2 methylation could potentially favor uORF2 translation by positioning the scanning or migrating ribosomes near the uORF2 start codon. Regardless, both mechanisms lead to repressed translation of the downstream coding region of ATF4. The presence of this m^{6}A-marked checkpoint offers a failsafe mechanism to prevent the skipping ribosome to initiate the downstream main CDS under the nutrient-rich condition (Figure 5A). Upon amino acid starvation, however, decreased uORF2 methylation together with reduced TC availability allows continuous ribosome migration, thereby promoting reinitiation at downstream start codons. Under this scenario, uORF2 translation is also de-repressed, which explains the puzzling observation that increased uORF2 read density is associated with reduced uTIS peak (Figure 1A).

To test the possibility that m^{6}A controls start codon selection by retaining the scanning ribosome, we conducted a toeprinting assay based on primer extension inhibition by 80S ribosomes (Iwasaki et al., 2016). Capped mRNAs covering a portion of ATF4 5′ UTR were synthesized and incubated with rabbit reticulocyte lysates. Addition of cycloheximide (CHX) prevents elongation but allows the assembly of 80S ribosomes at potential start codons. The position of 80S ribosomes is determined by the size of reverse transcription products extended from an FAM-labeled probe annealed to the 3′ end of mRNA. In the absence of CHX, only the full-length product was detectable as expected

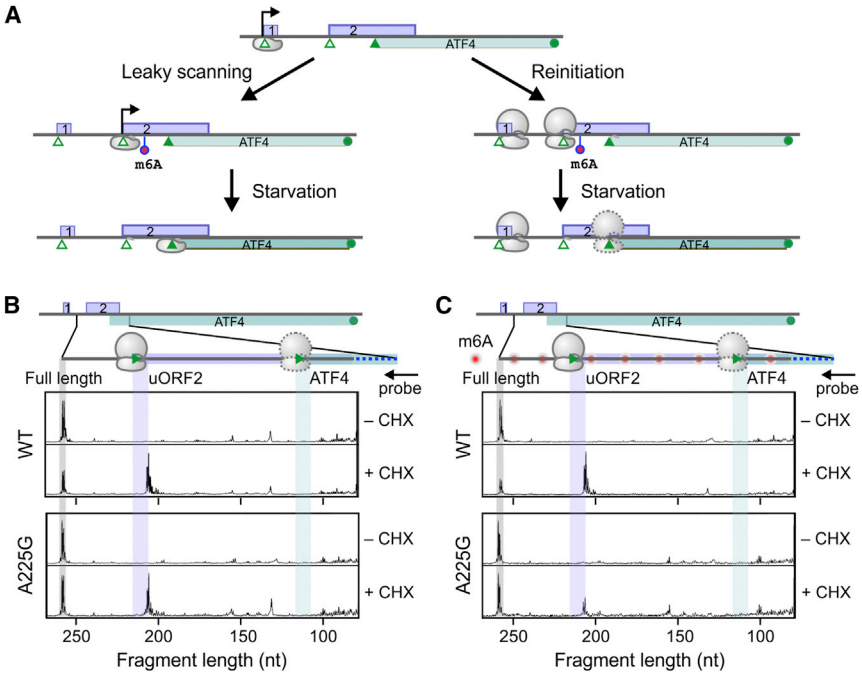

Figure 5. uORF2 Methylation Influences Start Codon Selection

(A) Schematic of uORF2 translation via leaky scanning (left panel) or reinitiation (right panel) influenced by uORF2 methylation.

(B) Toeprinting analysis using synthesized mRNAs with or without uORF2 mutation (A225G). Capped mRNAs were incubated in rabbit reticular lysates in the presence of cycloheximide. Expected positions corresponding to full length, uORF2 start codon, and the start codon of the main CDS are highlighted.

(C) Toeprinting analysis as in (B) using synthesized mRNAs incorporated with m^6A.

(Figure 5B). Presence of CHX resulted in a prominent peak corresponding to the uORF2 start codon. Similar to QTI-seq, toeprinting also failed to detect the main CDS start codon. Intriguingly, random m^6A incorporation increased the ribosome density at the uORF2 start codon (~2-fold) with a corresponding decrease of the full length (Figure 5C). This result suggests a strong retention of the 80S ribosome assembled at the start codon by m^6A. Alternatively, mRNA methylation may promote ribosome migration by disrupting secondary structures (Liu et al., 2015). To determine the site-specific effect of methylation, we introduced A225G mutation into the template. Eliminating m^6A at this position resulted in a marked reduction of the 80S ribosome at the uORF2 start codon (>5-fold) (Figure 5C). Taken together with the Fluc reporter bearing the same mutation (Figure 4C), it is clear that 5′ UTR methylation acts to impede ribosome migration, thereby increasing the probability of selecting upstream start codons that otherwise would be skipped.

5′ UTR Methylation Influences Global Alternative Translation

Previous studies, including ours, reported widespread alternative translation under different growth conditions, although the underlying mechanism remained elusive (Gao et al., 2015). Given the dynamic 5′ UTR methylation in response to nutrient starvation, it is possible that differential m^6A modification controls alternative start codon selection by influencing the ribosome scanning process. We first conducted m^6A-seq to illustrate the m^6A landscape in cells before and after nutrient deprivation. We observed a general increase of methylation in the 5′ UTR and a corresponding decrease of m^6A levels after the start codon (Figure 6A). This regional response is likely a consequence of distinct RNA-binding features between methyltransferases and demethylases. Indeed, direct comparison of PAR-CLIP datasets revealed that ALKBH5 preferentially binds to the CDS shortly after the start codon, whereas the METTL3-binding sites uniformly cover both the CDS and 3′ UTR (Figure S4B).

To interrogate whether the changes of mRNA methylation in the vicinity of start codons are correlated with TIS selection, we analyzed QTI-seq and m^6A-seq datasets in parallel. For transcripts without uTIS codons, hierarchical clustering revealed coordinated changes of ribosome density and m^6A levels around the annotated start codon (aTIS) (Spearman coefficient = 0.262, p = 0.008) (Figure 6B, left panel). The parallel response strongly suggests that mRNA methylation at the start codon region controls the ribosome dwell time at the aTIS. As a typical example, the gene encoding the lysosomal processing protein COPB2 underwent a clear reduction of m^6A downstream of the aTIS upon nutrient starvation (Figure 6C). As a result, the TIS peak captured by QTI-seq was substantially decreased (>5-fold). Notably, the reduced aTIS density led to an increase of ribosome occupancy along the CDS, supporting the notion that the lowered ribosome density at the start codon was not due to the inhibition of translation initiation. Instead, it suggests a previously unappreciated mechanism by which m^6A controls translation efficiency by retaining initiating ribosomes.

For transcripts bearing multiple TISs, however, the correlation between the changes of aTIS density and m^6A levels was weak (Spearman coefficient = 0.016, p = 0.913) (Figure 6B, right panel). This was rather expected because, according to the leaky scanning model, active translation of uORFs is believed to suppress the translation potential of the main ORFs. If 5′ UTR methylation favors uTIS selection by retaining the scanning ribosome, this would lower the leaky scanning probability and subsequently suppress the translation of the downstream ORF. Notably, many uORFs in 5′ UTRs are initiated from non-AUG start codons, such as CUG (Ingolia et al., 2011; Lee et al., 2012). We reasoned that 5′ UTR methylation, via retaining the scanning ribosome, could promote the selection of non-canonical TISs within the non-optimal sequence context. Indeed, among all the uTISs captured by QTI-seq, the majority of uTIS codons bearing downstream m^6A modification have relatively higher TIS signals (Figure 6D). Increased 5′ UTR methylation particularly increases

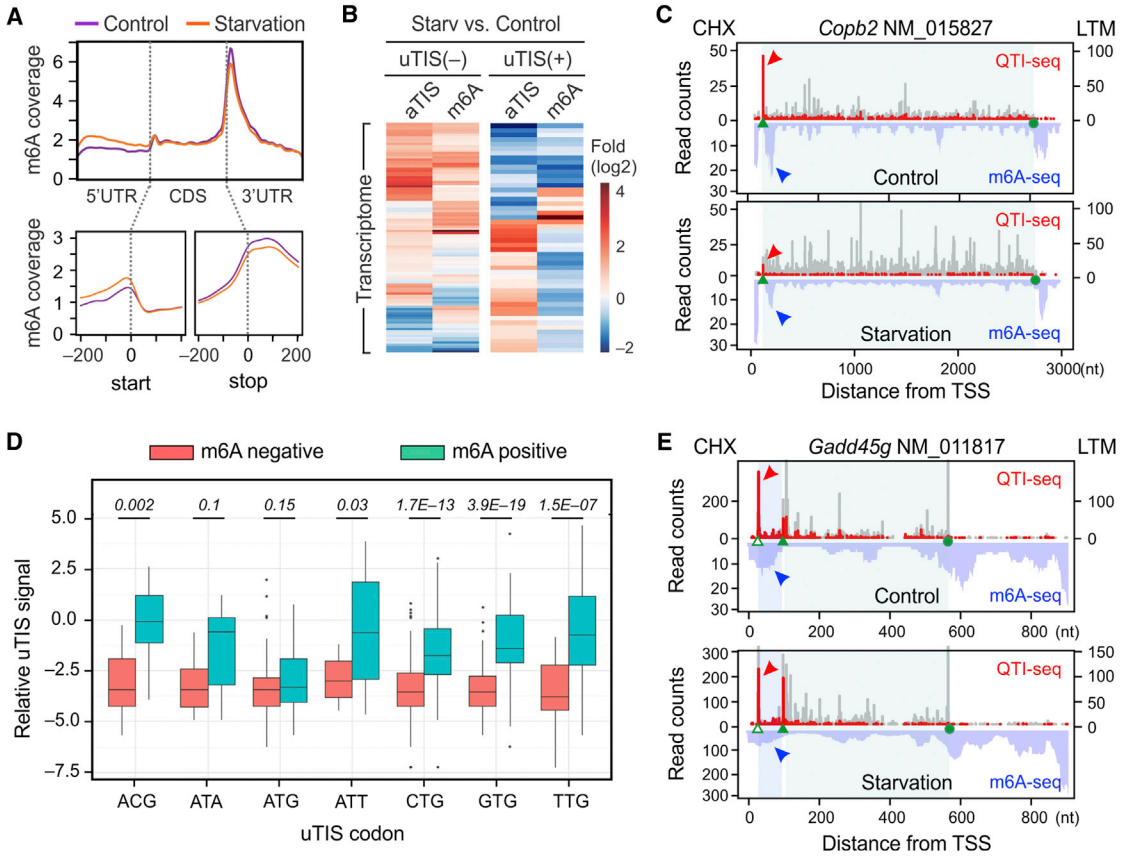

Figure 6. m^{6}A Guides Global Alternative Translation

(A) Metagene profiles of m^{6}A distribution across the transcriptome of MEF cells with or without amino acid starvation. The top panel shows normalized mRNA regions, while the bottom panel shows the distance around start and stop codons.

(B) Heatmap of fold changes of aTIS density and local m^{6}A levels (between –20 and + 60 nt) in response to amino acid starvation. Transcripts with or without uTIS are separated followed by hierarchical clustering.

(C) A representative example (*Copb2*) of genes showing coordinated changes of aTIS density and downstream m^{6}A levels in response to amino acid starvation.

(D) uTIS codons identified by QTI-seq under the normal growth condition are grouped based on positive or negative m^{6}A signals. Relative uTIS densities of individual TIS codons are plotted in a boxplot. p values (Wilcoxon test) are shown above each box.

(E) A representative example (*Gadd45 g*) of genes showing decreased uTIS density and increased aTIS density as a result of changed m^{6}A levels in response to amino acid starvation.

the signal of non-AUG codons. We previously reported that a starvation-responsive gene, *Gadd45 g*, bears a non-canonical uTIS codon, CUG, and mutating this uTIS abolished the starvation responsiveness (Gao et al., 2015). Re-analyzing QTI-seq together with m^{6}A-seq, we found that *Gadd45 g* employed the similar mechanism as *Atf4* in translational regulation (Figure 6E). Upon amino acid starvation, while *Atf4* relies on reduced uORF2 methylation to promote translation of the main CDS, *Gadd45 g* enhances the translation of the main CDS by reducing 5′ UTR methylation. Therefore, m^{6}A-guided alternative translation has a much broader effect during ISR.

Alternative Translation in Liver-Specific *Fto* Transgenic Mice

Acting as a master regulator of ISR, the transcription factor ATF4 has been shown to play a key role in many physiological processes, including metabolic homeostasis (Ameri and Harris, 2008). *Atf4*-deficient mice are lean and resist diet-induced diabetes (Seo et al., 2009). This phenotype is reminiscent of *Fto* knockout mice that were reported to have slow growth and reduced fat mass (Fischer et al., 2009). Although new studies proposed different genetic interpretation (Smemo et al., 2014), transgenic mice with FTO overexpression exhibited increased food intake and obesity (Church et al., 2010). It is possible that the FTO-associated metabolic phenotype is attributed in part to ATF4 dysregulation. In particular, ectopic expression of FTO in MEF cells promoted ATF4 levels following amino acid starvation, and this was not due to altered mRNA abundancy (Figure S5). This finding prompted us to investigate the physiological role of mRNA methylation *in vivo* using an FTO transgenic mouse model. To minimize the whole-body phenotypic complication, we created conditional *Fto* transgenic mice (Figure S6). Liver-specific FTO transgenic mice were then achieved by crossing the *Fto*^{Tg} mouse with a Cre recombinase-expressing mouse

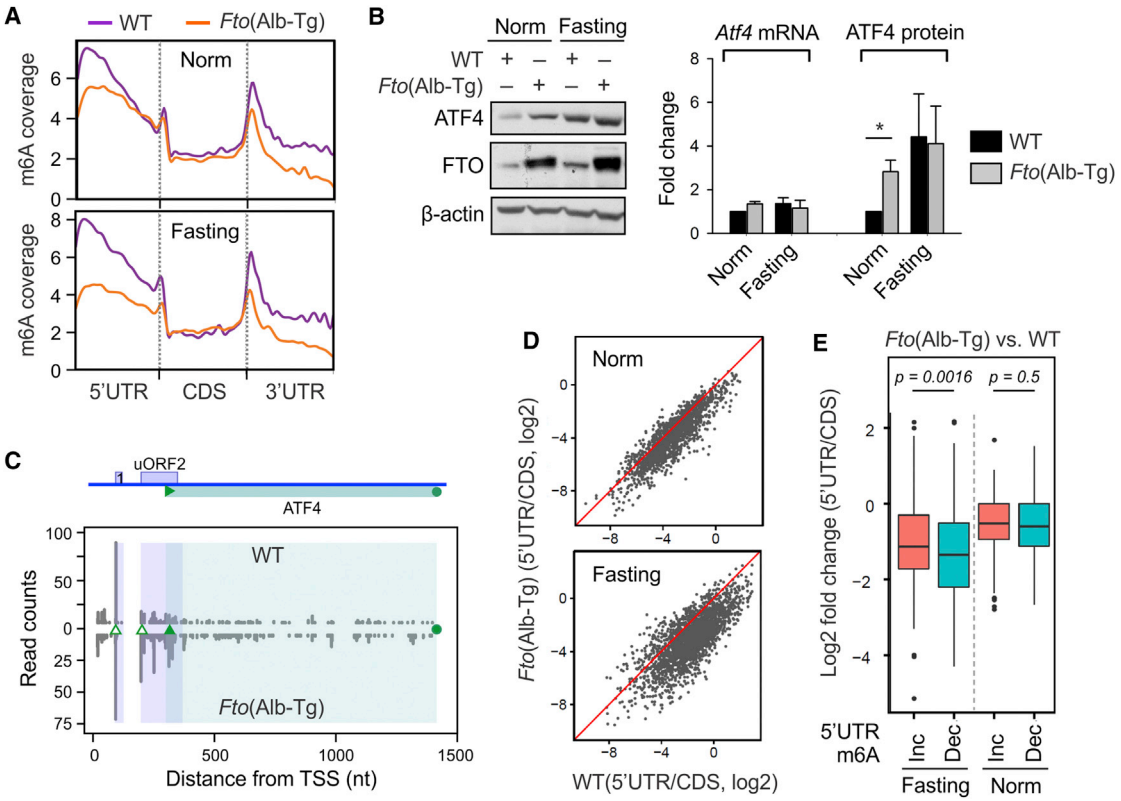

Figure 7. Alternative Translation in Liver-Specific *Fto* Transgenic Mice

(A) Metagene profiles of m^{6}A distribution across the transcriptome of liver lysates derived from wild-type or *Fto*$^{Alb\text{-}Tg}$ mice under well-fed (top panel) or overnight fasting (bottom panel) conditions.

(B) Immunoblotting of liver lysates derived from wild-type or *Fto*$^{Alb\text{-}Tg}$ mice under well-fed or overnight fasting conditions. The right panel shows the relative *Atf4* mRNA levels obtained by qPCR, as well as ATF4 protein levels quantified by densitometry and normalized to β-actin. Error bars, mean ± SEM; n = 3 biological replicates. *p < 0.05.

(C) Ribo-seq reads mapped to *Atf4* of liver lysates derived from wild-type or *Fto*$^{Alb\text{-}Tg}$ mice are presented in bar graphs.

(D) Scatterplots showing the correlation of regional ribosome density (5′ UTR versus CDS) between wild-type or *Fto*$^{Alb\text{-}Tg}$ mice under normal feeding (top panel) and overnight fasting (bottom panel) conditions.

(E) Boxplots showing changes of regional ribosome density (5′ UTR versus CDS) for transcripts with differential 5′ UTR methylation in liver lysates derived from *Fto*$^{Alb\text{-}Tg}$ mice. Dec and Inc refer to mRNAs with relatively decreased and increased 5′ UTR methylation, respectively. p values (Wilcoxon test) are shown above each box.

See also Figures S5–S7.

under the control of albumin promoter (Alb-Cre). The resultant *Fto*$^{Alb\text{-}Tg}$ mice were anatomically normal and reached adulthood without overt phenotypes. The tissue specificity of FTO overexpression was confirmed by immunoblotting that showed approximately 3-fold overexpression of FTO in liver, but not heart tissues (Figure S7A).

We next conducted m^{6}A-seq to illustrate the landscape of methylation in liver lysates with or without FTO overexpression. In comparison to MEF cells, liver lysates exhibited much higher m^{6}A levels in the 5′ UTR (Figure 7A). Such discrepancy could reflect the relatively nutrient-limiting environment within the solid tissues. It is possible that translational control of messages in solid tissues is more susceptible to changes of mRNA methylation than cells in culture. A recent study suggested that FTO preferentially demethylates m^{6}Am at the 5′ end of mRNA (Mauer et al., 2017). Indeed, we found that the 5′ end methylation was mostly reduced in liver lysates from *Fto*$^{Alb\text{-}Tg}$ mice (Figure 7A). However, the m^{6}A levels in other regions were also decreased, supporting the notion that FTO also targets internal m^{6}A sites. Surprisingly, the liver lysates derived from *Fto*$^{Alb\text{-}Tg}$ mice showed higher ATF4 protein levels than the wild-type even under the normal feeding condition (Figure 7B). Although the basal level of *Atf4* mRNA was slightly elevated, the much greater increase in protein levels of ATF4 suggests that mRNA methylation-regulated translation holds true *in vivo*. The enhanced ATF4 translation was further confirmed by Ribo-seq that revealed increased ribosome density in the main CDS of *Atf4* in *Fto*$^{Alb\text{-}Tg}$ liver lysates (Figure 7C). Once again, the uORF2 read density was also evidently increased under FTO overexpression. Therefore, in solid tissues like liver, the altered methylation contributes to the regulation of ATF4 translation.

We next examined whether *Fto*$^{Alb\text{-}Tg}$ mice still maintained the proper responsiveness to nutrient starvation, despite the elevated ATF4 levels under the normal fed condition. Following

overnight fasting, both wild-type and *Fto*$^{Alb\text{-}Tg}$ mice showed collapsed polysome in liver lysates (Figure S7B). As expected, wild-type mice responded to food withdrawal by elevating both mRNA and protein levels of ATF4 (Figures 7B and S7C). For *Fto*$^{Alb\text{-}Tg}$ mice, we observed a further increase of ATF4 protein levels in fasted liver despite the minimal change of mRNA abundance (Figure 7B). Given the large reduction of 5′ UTR methylation under FTO overexpression (Figure 7A), we next interrogated the relationship between FTO overexpression and alternative translation *in vivo*. In agreement with the finding that 5′ UTR methylation promotes uTIS selection (Figure 6D), FTO overexpression resulted in reduced 5′ UTR ribosome density relative to CDS (Figure 7D). This feature becomes more evident under the fasting condition, which is consistent with the much larger difference seen in the 5′ UTR methylation after overnight fasting. The quantitative difference of 5′ UTR read density was further confirmed when the 3′ UTR read density was considered as an internal control (Figure S7D). To confirm the regional effects of 5′ UTR methylation, we stratified transcripts based on 5′ UTR methylation changes. For transcripts with decreased 5′ UTR m^{6}A levels in *Fto*(Alb-Tg) samples, we observed a reduced 5′ UTR/CDS ratio (Figure 7E). Once again, this feature becomes more evident under the fasting condition ($p = 0.00043$, Wilcoxon test). Together, these results suggest that dynamic 5′ UTR methylation not only facilitates selective translation of ATF4, but also contributes to global alternative translation during ISR.

DISCUSSION

Classically, stress-induced enhancement of ATF4 expression is known to occur via increased translation efficiency of existing ATF4 mRNA. The current view holds that the timing of TC acquiring by reinitiating ribosomes is solely responsible for the efficiency of ATF4 translation. Supporting this notion, the gene architecture of ATF4 uORFs and the distance separating uORFs and the main CDS are highly conserved among vertebrates (Vattem and Wek, 2004). However, physiological fluctuations of TC concentrations do not seem to give rise to stochastic ATF4 expression (Lu et al., 2004). In addition, it is puzzling to find that the uORF2 translation is not necessarily suppressed during ISR-induced ATF4 activation (Starck et al., 2016). Additional mechanisms are likely in place to tightly control ATF4 reinitiation in response to reduced TC availability during ISR. In this study, we demonstrate that dynamic 5′ UTR methylation modulates ATF4 translation by controlling the dwell time of scanning ribosomes on uORF2. Together with the eIF2α signaling pathway, mRNA methylation in the form of m^{6}A reconfigures the ISR at cellular and organismal levels.

Much like the epigenetic modification of DNA and histones, m^{6}A modification of mRNA is reversible (Jia et al., 2011; Zheng et al., 2013). Although the majority of m^{6}A is enriched near stop codons, the 5′ UTR undergoes more dynamic modification in response to different growth conditions (Dominissini et al., 2012). This is likely due to the distinct substrate specificity for m^{6}A "erasers" compared to the "writers." While the latter relies on the consensus sequence motif to install m^{6}A, the former tends to recognize conformational markers signified by m^{6}A (Zou et al., 2016). Notably, ALKBH5 appears to be a stress-responsive gene. For instance, hypoxia-induced ALKBH5 targets methylated NANOG mRNA in breast cancer cells (Zhang et al., 2016). In response to nutrient starvation, we observed specific recruitment of ALKBH5 to ATF4 mRNA as evidenced by quantitative proteomic analysis. As a result, the uORF2 methylation was reduced relative to other regions of ATF4. How exactly the substrate and regional specificity is achieved awaits further investigation. It appears that dynamic uORF2 methylation plays an important role in achieving selective translation of ATF4 during ISR.

We previously demonstrated that m^{6}A modification in the 5′ UTR enables cap-independent translation (Meyer et al., 2015; Zhou et al., 2015). However, the translation of ATF4 uORF1 seems to follow the "classic" cap-dependent mechanism. It is thus intriguing to find that 5′ UTR methylation also regulates alternative translation. A key to alternative translation is the start codon selection. It is commonly assumed that the first AUG codon that the scanning ribosome encounters serves as the start site for translation. However, one or more potential initiation sites could exist upstream or downstream of the main start codon (Iacono et al., 2005). For transcripts with multiple start sites, the TIS stringency is thought to be determined by the sequence context surrounding the start codon. However, the static sequence feature cannot fully explain the altered uORF occupancy under various stress conditions such as nutrient starvation. We show here that dynamic 5′ UTR methylation finely tunes uORF translation by influencing start codon selection. The mechanism whereby m^{6}A modification in the 5′ UTR regulates TIS recognition remains to be fully defined. At least three possibilities exist. First, m^{6}A could interact directly with eIF3a, an essential component of the pre-initiation complex, to slow down the scanning process. Recent studies using *in vitro* UV crosslinking demonstrated direct interaction between m^{6}A and eIF3a (Meyer et al., 2015). In addition, a considerable amount of m^{6}A peaks overlap with eIF3a-binding sites on mRNAs as revealed by PAR-CLIP. Second, site-specific m^{6}A modification could alter local mRNA secondary structures that potentially create road blocks for scanning ribosomes. Indeed, a recent study demonstrated that m^{6}A acts as a structural switch for a substantial amount of RNA molecules (Liu et al., 2015). Finally, m^{6}A could recruit certain "readers" to 5′ UTR and the presence of RNP complexes potentially delays the scanning process. Interestingly, m^{6}A installed to the nascent mRNA chains has been recently found to negatively regulate translation, presumably by delaying ribosome movement (Slobodin et al., 2017). Impediments to ribosome scanning by stable hairpin or RBPs has long been described to enhance the translation from uORFs that otherwise would be skipped (Kozak, 1990; Medenbach et al., 2011). In this study, we provide evidence that many non-AUG start codons are associated with local methylation. By influencing ribosomal scanning and the subsequent TIS selection, 5′ UTR methylation broadly affects alternative translation during ISR. In the case of ATF4, clearance of the uORF2 roadblock not only allows uORF2 translation to occur, but also enables translation of the main CDS of ATF during reinitiation.

The bZip transcription factor ATF4 is expressed constitutively only at low levels but becomes rapidly induced during ISR.

However, ATF4 is expressed at relatively high levels throughout embryonic and postnatal testis development (Muir et al., 2008). ATF4 null mutant mice had adult testis phenotypes of reduced spermatogenic capacity. Surprisingly, ALKBH5-deficient male mice are characterized by impaired fertility (Zheng et al., 2013). Given the deficient ATF4 translation in the absence of ALKBH5, it is likely that the impaired alternative translation represents a common mechanism deeply rooted in the phenotypes of mice lacking ALKBH5. In contrast to ALKBH5 that is highly expressed in testes, the m^{6}A demethylase FTO is prevalent in somatic tissues such as neuron. The metabolic phenotype associated with FTO null or transgenic mice could also be interpreted as a consequence of dysregulated ATF4, at least partially. For instance, FTO depletion led to impaired adipogenesis *in vitro* and *in vivo* (Zhao et al., 2014). Similarly, knockdown ATF4 in 3T3-L1 cells also inhibits adipogenesis (Chen et al., 2016). In addition, ATF4 has been shown to license C/EBPβ activity in human mesenchymal stem cells primed for adipogenesis (Cohen et al., 2015). Using MEF cells in culture and liver-specific FTO transgenic mice, we provide solid evidence that altered mRNA methylation influences alternative translation as exemplified by ATF4 expression. Given the broad function of ATF4 in metabolic homeostasis (Seo et al., 2009), our findings encourage us to reconsider the mechanistic interpretation of phenotypes associated with animal models with disrupted m^{6}A methylation machinery.

Broadly, the principle of mRNA methylation in translational control might be interwoven with other functions of m^{6}A on RNA biology, such as mRNA stability and splicing (Dominissini et al., 2012; Wang et al., 2014). Given the fundamental role of m^{6}A in physiological processes such as stem cell differentiation (Batista et al., 2014; Geula et al., 2015), the involvement of translational control in these cellular processes merits further investigation. In conclusion, our results reveal that 5′ UTR methylation in the form of m^{6}A acts as a dynamic regulator in alternative translation. The insights obtained from this study further advance our understanding of physiological roles of mRNA methylation in general and additional aspects of translational control in response to stress.

STAR★METHODS

Detailed methods are provided in the online version of this paper and include the following:

- KEY RESOURCES TABLE
- CONTACT FOR REAGENT AND RESOURCE SHARING
- EXPERIMENTAL MODEL AND SUBJECT DETAILS
  - Cell lines and reagents
  - FTO transgenic mice
- METHOD DETAILS
  - Plasmid constructions
  - Lentiviral shRNAs
  - Amino acid starvation treatment
  - SILAC
  - Immunoblotting
  - Real-time quantitative PCR
  - m^{6}A dot blot
  - Dual-luciferase assay
  - Toeprinting
  - *Tth*-mediated m^{6}A site-specific detection
  - Polysome profiling analysis
  - RNA-seq and m^{6}A–seq
  - QTI-seq and Ribo-seq
  - cDNA library construction
  - Deep sequencing
- QUANTIFICATION AND STATISTICAL ANALYSIS
  - m^{6}A-Seq coverage analysis
  - Ribosome profiling analysis
  - Heatmap of aTIS density change and local m^{6}A level change
  - Impact of 5′ UTR m^{6}A signal on ribosome occupancy
  - PAR-CLIP analysis
- DATA AND SOFTWARE AVAILABILITY

SUPPLEMENTAL INFORMATION

Supplemental Information includes seven figures and one table and can be found with this article online at https://doi.org/10.1016/j.molcel.2018.01.019.

ACKNOWLEDGMENTS

We'd like to thank Qian lab members for helpful discussion. We also thank Dr. Ronald C. Wek (Indiana University School of Medicine) for providing us with the ATF4 reporter construct. We are grateful to Cornell University Life Sciences Core Laboratory Center for performing deep sequencing. This work was supported by grants to S.-B.Q. from the NIH (R01AG042400), the United States Department of Defense (W81XWH-14-1-0068), and HHMI Faculty Scholar (55108556).

AUTHOR CONTRIBUTIONS

J.Z. and S.-B.Q. conceived the project and designed the study. J.Z. performed most of the experiments. X.E.S. performed SILAC experiments. J.W. and Y.M. analyzed the sequencing data. X.-M.L. and X.Y. assisted reporter assays. X.Z. helped with mouse studies. M.E.H. and J.C.B. created *Fto* transgenic mice. S.-B.Q. wrote the manuscript. All authors discussed results and edited the manuscript.

DECLARATION OF INTERESTS

The authors declare no competing interests.

Received: March 30, 2017
Revised: October 20, 2017
Accepted: January 12, 2018
Published: February 8, 2018

REFERENCES

Alarcón, C.R., Goodarzi, H., Lee, H., Liu, X., Tavazoie, S., and Tavazoie, S.F. (2015). HNRNPA2B1 is a mediator of m(6)A-dependent nuclear RNA processing events. Cell *162*, 1299–1308.

Ameri, K., and Harris, A.L. (2008). Activating transcription factor 4. Int. J. Biochem. Cell Biol. *40*, 14–21.

Baltz, A.G., Munschauer, M., Schwanhäusser, B., Vasile, A., Murakawa, Y., Schueler, M., Youngs, N., Penfold-Brown, D., Drew, K., Milek, M., et al. (2012). The mRNA-bound proteome and its global occupancy profile on protein-coding transcripts. Mol. Cell *46*, 674–690.

Batista, P.J., Molinie, B., Wang, J., Qu, K., Zhang, J., Li, L., Bouley, D.M., Lujan, E., Haddad, B., Daneshvar, K., et al. (2014). m(6)A RNA modification

controls cell fate transition in mammalian embryonic stem cells. Cell Stem Cell *15*, 707–719.

Bokar, J.A., Shambaugh, M.E., Polayes, D., Matera, A.G., and Rottman, F.M. (1997). Purification and cDNA cloning of the AdoMet-binding subunit of the human mRNA (N6-adenosine)-methyltransferase. RNA *3*, 1233–1247.

Chen, H., Yuan, R., Zhang, Y., Zhang, X., Chen, L., Zhou, X., Yuan, Z., Nie, Y., Li, M., Mo, D., and Chen, Y. (2016). ATF4 regulates SREBP1c expression to control fatty acids synthesis in 3T3-L1 adipocytes differentiation. Biochim. Biophys. Acta *1859*, 1459–1469.

Choi, J., Ieong, K.W., Demirci, H., Chen, J., Petrov, A., Prabhakar, A., O'Leary, S.E., Dominissini, D., Rechavi, G., Soltis, S.M., et al. (2016). N(6)-methyladenosine in mRNA disrupts tRNA selection and translation-elongation dynamics. Nat. Struct. Mol. Biol. *23*, 110–115.

Church, C., Moir, L., McMurray, F., Girard, C., Banks, G.T., Teboul, L., Wells, S., Brüning, J.C., Nolan, P.M., Ashcroft, F.M., and Cox, R.D. (2010). Overexpression of Fto leads to increased food intake and results in obesity. Nat. Genet. *42*, 1086–1092.

Cohen, D.M., Won, K.J., Nguyen, N., Lazar, M.A., Chen, C.S., and Steger, D.J. (2015). ATF4 licenses C/EBPβ activity in human mesenchymal stem cells primed for adipogenesis. eLife *4*, e06821.

Corcoran, D.L., Georgiev, S., Mukherjee, N., Gottwein, E., Skalsky, R.L., Keene, J.D., and Ohler, U. (2011). PARalyzer: definition of RNA binding sites from PAR-CLIP short-read sequence data. Genome Biol. *12*, R79.

Dever, T.E., Feng, L., Wek, R.C., Cigan, A.M., Donahue, T.F., and Hinnebusch, A.G. (1992). Phosphorylation of initiation factor 2 alpha by protein kinase GCN2 mediates gene-specific translational control of GCN4 in yeast. Cell *68*, 585–596.

Dominissini, D., Moshitch-Moshkovitz, S., Schwartz, S., Salmon-Divon, M., Ungar, L., Osenberg, S., Cesarkas, K., Jacob-Hirsch, J., Amariglio, N., Kupiec, M., et al. (2012). Topology of the human and mouse m6A RNA methylomes revealed by m6A-seq. Nature *485*, 201–206.

Fischer, J., Koch, L., Emmerling, C., Vierkotten, J., Peters, T., Brüning, J.C., and Rüther, U. (2009). Inactivation of the Fto gene protects from obesity. Nature *458*, 894–898.

Fu, Y., Dominissini, D., Rechavi, G., and He, C. (2014). Gene expression regulation mediated through reversible m^6A RNA methylation. Nat. Rev. Genet. *15*, 293–306.

Gao, X., Wan, J., Liu, B., Ma, M., Shen, B., and Qian, S.B. (2015). Quantitative profiling of initiating ribosomes in vivo. Nat. Methods *12*, 147–153.

Gebauer, F., and Hentze, M.W. (2004). Molecular mechanisms of translational control. Nat. Rev. Mol. Cell Biol. *5*, 827–835.

Geula, S., Moshitch-Moshkovitz, S., Dominissini, D., Mansour, A.A., Kol, N., Salmon-Divon, M., Hershkovitz, V., Peer, E., Mor, N., Manor, Y.S., et al. (2015). Stem cells. m6A mRNA methylation facilitates resolution of naïve pluripotency toward differentiation. Science *347*, 1002–1006.

Harding, H.P., Calfon, M., Urano, F., Novoa, I., and Ron, D. (2002). Transcriptional and translational control in the mammalian unfolded protein response. Annu. Rev. Cell Dev. Biol. *18*, 575–599.

Hinnebusch, A.G. (2014). The scanning mechanism of eukaryotic translation initiation. Annu. Rev. Biochem. *83*, 779–812.

Hinnebusch, A.G., Ivanov, I.P., and Sonenberg, N. (2016). Translational control by 5′-untranslated regions of eukaryotic mRNAs. Science *352*, 1413–1416.

Iacono, M., Mignone, F., and Pesole, G. (2005). uAUG and uORFs in human and rodent 5'untranslated mRNAs. Gene *349*, 97–105.

Ingolia, N.T., Lareau, L.F., and Weissman, J.S. (2011). Ribosome profiling of mouse embryonic stem cells reveals the complexity and dynamics of mammalian proteomes. Cell *147*, 789–802.

Iwasaki, S., Floor, S.N., and Ingolia, N.T. (2016). Rocaglates convert DEAD-box protein eIF4A into a sequence-selective translational repressor. Nature *534*, 558–561.

Jackson, R.J., Hellen, C.U., and Pestova, T.V. (2010). The mechanism of eukaryotic translation initiation and principles of its regulation. Nat. Rev. Mol. Cell Biol. *11*, 113–127.

Jia, G., Fu, Y., Zhao, X., Dai, Q., Zheng, G., Yang, Y., Yi, C., Lindahl, T., Pan, T., Yang, Y.G., and He, C. (2011). N6-methyladenosine in nuclear RNA is a major substrate of the obesity-associated FTO. Nat. Chem. Biol. *7*, 885–887.

Kozak, M. (1990). Downstream secondary structure facilitates recognition of initiator codons by eukaryotic ribosomes. Proc. Natl. Acad. Sci. USA *87*, 8301–8305.

Lee, S., Liu, B., Lee, S., Huang, S.X., Shen, B., and Qian, S.B. (2012). Global mapping of translation initiation sites in mammalian cells at single-nucleotide resolution. Proc. Natl. Acad. Sci. USA *109*, E2424–E2432.

Liu, B., and Qian, S.B. (2014). Translational reprogramming in cellular stress response. Wiley Interdiscip. Rev. RNA *5*, 301–315.

Liu, J., Yue, Y., Han, D., Wang, X., Fu, Y., Zhang, L., Jia, G., Yu, M., Lu, Z., Deng, X., et al. (2014). A METTL3-METTL14 complex mediates mammalian nuclear RNA N6-adenosine methylation. Nat. Chem. Biol. *10*, 93–95.

Liu, N., Dai, Q., Zheng, G., He, C., Parisien, M., and Pan, T. (2015). N(6)-methyladenosine-dependent RNA structural switches regulate RNA-protein interactions. Nature *518*, 560–564.

Lu, P.D., Harding, H.P., and Ron, D. (2004). Translation reinitiation at alternative open reading frames regulates gene expression in an integrated stress response. J. Cell Biol. *167*, 27–33.

Mauer, J., Luo, X., Blanjoie, A., Jiao, X., Grozhik, A.V., Patil, D.P., Linder, B., Pickering, B.F., Vasseur, J.J., Chen, Q., et al. (2017). Reversible methylation of m6Am in the 5′ cap controls mRNA stability. Nature *541*, 371–375.

Medenbach, J., Seiler, M., and Hentze, M.W. (2011). Translational control via protein-regulated upstream open reading frames. Cell *145*, 902–913.

Meyer, K.D., and Jaffrey, S.R. (2014). The dynamic epitranscriptome: N6-methyladenosine and gene expression control. Nat. Rev. Mol. Cell Biol. *15*, 313–326.

Meyer, K.D., Saletore, Y., Zumbo, P., Elemento, O., Mason, C.E., and Jaffrey, S.R. (2012). Comprehensive analysis of mRNA methylation reveals enrichment in 3′ UTRs and near stop codons. Cell *149*, 1635–1646.

Meyer, K.D., Patil, D.P., Zhou, J., Zinoviev, A., Skabkin, M.A., Elemento, O., Pestova, T.V., Qian, S.B., and Jaffrey, S.R. (2015). 5′ UTR m(6)A promotes Cap-independent translation. Cell *163*, 999–1010.

Mueller, P.P., and Hinnebusch, A.G. (1986). Multiple upstream AUG codons mediate translational control of GCN4. Cell *45*, 201–207.

Muir, T., Wilson-Rawls, J., Stevens, J.D., Rawls, A., Schweitzer, R., Kang, C., and Skinner, M.K. (2008). Integration of CREB and bHLH transcriptional signaling pathways through direct heterodimerization of the proteins: role in muscle and testis development. Mol. Reprod. Dev. *75*, 1637–1652.

Ping, X.L., Sun, B.F., Wang, L., Xiao, W., Yang, X., Wang, W.J., Adhikari, S., Shi, Y., Lv, Y., Chen, Y.S., et al. (2014). Mammalian WTAP is a regulatory subunit of the RNA N6-methyladenosine methyltransferase. Cell Res. *24*, 177–189.

Seo, J., Fortuno, E.S., 3rd, Suh, J.M., Stenesen, D., Tang, W., Parks, E.J., Adams, C.M., Townes, T., and Graff, J.M. (2009). Atf4 regulates obesity, glucose homeostasis, and energy expenditure. Diabetes *58*, 2565–2573.

Skabkin, M.A., Skabkina, O.V., Hellen, C.U., and Pestova, T.V. (2013). Reinitiation and other unconventional posttermination events during eukaryotic translation. Mol. Cell *51*, 249–264.

Slobodin, B., Han, R., Calderone, V., Vrielink, J.A.F.O., Loayza-Puch, F., Elkon, R., and Agami, R. (2017). Transcription impacts the efficiency of mRNA translation via co-transcriptional N6-adenosine methylation. Cell *169*, 326–337.e12.

Smemo, S., Tena, J.J., Kim, K.H., Gamazon, E.R., Sakabe, N.J., Gómez-Marín, C., Aneas, I., Credidio, F.L., Sobreira, D.R., Wasserman, N.F., et al. (2014). Obesity-associated variants within FTO form long-range functional connections with IRX3. Nature *507*, 371–375.

Sonenberg, N., and Hinnebusch, A.G. (2007). New modes of translational control in development, behavior, and disease. Mol. Cell *28*, 721–729.

Sonenberg, N., and Hinnebusch, A.G. (2009). Regulation of translation initiation in eukaryotes: mechanisms and biological targets. Cell *136*, 731–745.

Starck, S.R., Tsai, J.C., Chen, K., Shodiya, M., Wang, L., Yahiro, K., Martins-Green, M., Shastri, N., and Walter, P. (2016). Translation from the 5′ untranslated region shapes the integrated stress response. Science *351*, aad3867.

Trapnell, C., Pachter, L., and Salzberg, S.L. (2009). TopHat: discovering splice junctions with RNA-seq. Bioinformatics *25*, 1105–1111.

Trapnell, C., Williams, B.A., Pertea, G., Mortazavi, A., Kwan, G., van Baren, M.J., Salzberg, S.L., Wold, B.J., and Pachter, L. (2010). Transcript assembly and quantification by RNA-seq reveals unannotated transcripts and isoform switching during cell differentiation. Nat. Biotechnol. *28*, 511–515.

Vattem, K.M., and Wek, R.C. (2004). Reinitiation involving upstream ORFs regulates ATF4 mRNA translation in mammalian cells. Proc. Natl. Acad. Sci. USA *101*, 11269–11274.

Wang, X., Lu, Z., Gomez, A., Hon, G.C., Yue, Y., Han, D., Fu, Y., Parisien, M., Dai, Q., Jia, G., et al. (2014). N6-methyladenosine-dependent regulation of messenger RNA stability. Nature *505*, 117–120.

Wang, X., Zhao, B.S., Roundtree, I.A., Lu, Z., Han, D., Ma, H., Weng, X., Chen, K., Shi, H., and He, C. (2015). N(6)-methyladenosine modulates messenger RNA translation efficiency. Cell *161*, 1388–1399.

Wek, R.C., Jiang, H.Y., and Anthony, T.G. (2006). Coping with stress: eIF2 kinases and translational control. Biochem. Soc. Trans. *34*, 7–11.

Xiao, W., Adhikari, S., Dahal, U., Chen, Y.S., Hao, Y.J., Sun, B.F., Sun, H.Y., Li, A., Ping, X.L., Lai, W.Y., et al. (2016). Nuclear m(6)A reader YTHDC1 regulates mRNA splicing. Mol. Cell *61*, 507–519.

Xu, C., Liu, K., Tempel, W., Demetriades, M., Aik, W., Schofield, C.J., and Min, J. (2014). Structures of human ALKBH5 demethylase reveal a unique binding mode for specific single-stranded N6-methyladenosine RNA demethylation. J. Biol. Chem. *289*, 17299–17311.

Zhang, C., Samanta, D., Lu, H., Bullen, J.W., Zhang, H., Chen, I., He, X., and Semenza, G.L. (2016). Hypoxia induces the breast cancer stem cell phenotype by HIF-dependent and ALKBH5-mediated m^6A-demethylation of NANOG mRNA. Proc. Natl. Acad. Sci. USA *113*, E2047–E2056.

Zhao, X., Yang, Y., Sun, B.F., Shi, Y., Yang, X., Xiao, W., Hao, Y.J., Ping, X.L., Chen, Y.S., Wang, W.J., et al. (2014). FTO-dependent demethylation of N6-methyladenosine regulates mRNA splicing and is required for adipogenesis. Cell Res. *24*, 1403–1419.

Zheng, G., Dahl, J.A., Niu, Y., Fedorcsak, P., Huang, C.M., Li, C.J., Vågbø, C.B., Shi, Y., Wang, W.L., Song, S.H., et al. (2013). ALKBH5 is a mammalian RNA demethylase that impacts RNA metabolism and mouse fertility. Mol. Cell *49*, 18–29.

Zhou, J., Wan, J., Gao, X., Zhang, X., Jaffrey, S.R., and Qian, S.B. (2015). Dynamic m(6)A mRNA methylation directs translational control of heat shock response. Nature *526*, 591–594.

Zou, S., Toh, J.D., Wong, K.H., Gao, Y.G., Hong, W., and Woon, E.C. (2016). N(6)-methyladenosine: a conformational marker that regulates the substrate specificity of human demethylases FTO and ALKBH5. Sci. Rep. *6*, 25677.

STAR★METHODS

KEY RESOURCES TABLE

REAGENT or RESOURCE	SOURCE	IDENTIFIER
Antibodies		
Rabbit polyclonal anti-ATF4	Santa Cruz Biotechnology	Cat#SC-200; RRID: AB_2058752
Mouse monoclonal anti-β-actin	Sigma-Aldrich	Cat#A5441; RRID: AB_476744
Rabbit polyclonal anti-ALKBH5	Proteintech Group	Cat#16837-1-AP; RRID: AB_2242665
Mouse monoclonal anti-FTO	PhosphoSolutions	Cat#597-FTO; RRID: AB_2492098
Rabbit polyclonal anti-METTL3	Proteintech Group	Cat#15073-1-AP; RRID: AB_2142033
Rabbit polyclonal anti-METTL14	Sigma-Aldrich	Cat#HPA038002; RRID: AB_10672401
Rabbit monoclonal anti-eIF2α (D7D3) XP	Cell Signaling Technology	Cat#5324
Rabbit monoclonal anti-phospho-eIF2α (Ser51)(D9G8) XP	Cell Signaling Technology	Cat#3398
Rabbit monoclonal anti-S6 Ribosomal Protein	Cell Signaling Technology	Cat#2217; RRID: AB_331355
Rabbit polyclonal anti-RPL4	Proteintech Group	Cat#11302-1-AP; RRID: AB_2181909
Rabbit polyclonal anti-m^{6}A	Millipore	Cat#ABE572
Rabbit polyclonal anti-m^{6}A	Synaptic Systems	Cat#202 003; RRID: AB_2279214
Bacterial and Virus Strains		
DECIPHER pRSI9-U6-(sh)-UbiC-TagRFP-2A-Puro	Cellecta	N/A
Subcloning Efficiency DH5α Competent Cells	Invitrogen	Cat#18265-017
Chemicals, Peptides, and Recombinant Proteins		
Cycloheximide	Sigma-Aldrich	Cat#C7698
N^6-Methyladenosine 5′-monophosphate sodium salt	Sigma-Aldrich	Cat#M2780
HindIII	New England Biolabs	Cat#R0104L
XbaI	New England Biolabs	Cat#R0145L
Puromycin	Sigma-Aldrich	Cat#P7255
HBSS buffer	Lonza	Cat#10-527F
Fetal Bovine Serum, Dialyzed	Sigma-Aldrich	Cat#F0392
Yeast tRNA	Invitrogen	Cat#AM7119
SUPERase_In	Invitrogen	Cat#AM2696
TRIzol LS Reagent	Invitrogen	Cat#10296-028
Trizol Reagent	Invitrogen	Cat#15596-018
RNaseOUT Recombinant Ribonuclease Inhibitor	Invitrogen	Cat#10777-019
SYBR Gold nucleic acid gel stain	Invitrogen	Cat# S-11494
CircLigase ssDNA Ligase	Epicenter	Cat# CL4115K
Phusion* High-Fidelity DNA Polymerase	Thermo Fisher Scientific	Cat#F530L
Critical Commercial Assays		
QuikChange II XL Site-Directed Mutagenesis Kit	Agilent Technologies	Cat#200521
Affi-Gel Heparin Gel	Bio-rad	Cat#1536173
High Capacity cDNA Reverse Transcription Kit	Applied Biosystems	Cat#4368814
Power SYBR Green PCR Master Mix	Applied Biosystems	Cat#4368706
Dual-Luciferase Reporter Assay System	Promega	Cat#E1910
Rabbit Reticulocyte Lysate System, Nuclease Treated	Promega	Cat#L4960
SuperScript III Reverse Transcriptase	Thermo Fisher Scientific	Cat#18080-044
Hi-Di formamide	Thermo Fisher Scientific	Cat#4311320
GeneScan 500 LIZ dye Size Standard	Thermo Fisher Scientific	Cat#4322682
Dynabeads M-280 Streptavidin	Thermo Fisher Scientific	Cat#11206D
Dynabeads Oligo(dT)25	Thermo Fisher Scientific	Cat#61005

(*Continued on next page*)

Continued

REAGENT or RESOURCE	SOURCE	IDENTIFIER
Deposited Data		
Raw sequencing data	This paper	GEO: GSE102659
Re-analyzed Ribo-seq data	Gao et al., 2015	SRA: SRA160745
Re-analyzed PAR-CLIP data	Baltz et al., 2012; Ping et al., 2014	GEO: GSE38201 and GSE50580
Original images	Mendeley	https://doi.org/10.17632/p4kwsdgkck.2
Mouse genome, transcriptome, GRCm38.p4	Ensembl	http://www.ensembl.org/index.html
Experimental Models: Cell Lines		
Mouse: embryonic fibroblast cells	Laboratory of David J. Kwiatkowski	N/A
Human: Lenti-X 293T Cell Line	Clontech	Cat#632180
Experimental Models: Organisms/Strains		
Mouse: B6:FTO-Tg	This study	N/A
Oligonucleotides		
shRNA targeting sequence: ALKBH5: GCCTCAGGACATT AAGGAACG	This study	N/A
shRNA targeting sequence: FTO: GCTGAGGCAGTTCTG GTTTCA	This study	N/A
shRNA targeting sequence: METTL3: GCTACAGGATGAC GGCTTTCT	This study	N/A
shRNA targeting sequence: METTL14: GGATCAAAGGAA CCGTGAAGC	This study	N/A
shRNA targeting sequence: Scramble: AACAGTCGCGTT TGCGACTGG	This study	N/A
biotinylated oligo targeting the 3′UTR of human ATF4: 5′-Biotin-TEG-GTACAAGCACAAAGCACCTGACT-3′	This study	N/A
Primers for qPRC: ATF4-Fwd: 5′-CTTGATGTCCCCCTTC GACC-3′	This study	N/A
Primers for qPRC: ATF4-Rev: 5′- CTTGTCGCTGGAGAA CCCAT-3′	This study	N/A
Primers for qPRC: GAPDH-Fwd: 5′- CAAGGAGTAAGAAA CCCTGGA-3′	This study	N/A
Primers for qPRC: GAPDH-Rev: 5′- GGATGGAAATTGTG AGGGAGAT-3′	This study	N/A
Primers for Toeprinting assay: 5′-6-FAM-AATTGTTCCAG GAACCAG-3′	This study	N/A
Primers for reverse transcription in Library construction: MCA02, 5′-pCAGATCGTCGGACTGTAGAACTCTØCAAG CAGAAGACGGCATACGATTTTTTTTTTTTTTTTTTTVN-3′	Gao et al., 2015	N/A
Primers for reverse transcription in Library construction: LGT03, 5′-pGTGATCGTCGGACTGTAGAACTCTØCAAG CAGAAGACGGCATACGATTTTTTTTTTTTTTTTTTTVN-3′	Gao et al., 2015	N/A
Primers for reverse transcription in Library construction: YAG04, 5′-pAGGATCGTCGGACTGTAGAACTCTØCAAG CAGAAGACGGCATACGATTTTTTTTTTTTTTTTTTTVN-3′	Gao et al., 2015	N/A
Primers for reverse transcription in Library construction: HTC05, 5′-pTCGATCGTCGGACTGTAGAACTCTØCAAG CAGAAGACGGCATACGATTTTTTTTTTTTTTTTTTTVN-3′	Gao et al., 2015	N/A
Primers for amplification in Library construction: qNTI200: 5′-CAAGCAGAAGACGGCATA-3′	Gao et al., 2015	N/A

(*Continued on next page*)

Continued		
REAGENT or RESOURCE	SOURCE	IDENTIFIER
Primers for amplification in Library construction: qNTI201: 5′-AATGATACGGCGACCACCGAGATCTACACGTTCAGAGTTCTACAGTCCGACG-3′	Gao et al., 2015	N/A
Sequencing primer: 5′-CGACAGGTTCAGAGTTCTACAGTCCGACGATC-3′	Gao et al., 2015	N/A
Recombinant DNA		
pGL3 TK-ATF4 WT-5′-leader-Luciferase reporter	Vattem and Wek, 2004	N/A
pGL3 TK-ATF4 uORF2 deletion-Luciferase reporter	Vattem and Wek, 2004	N/A
pcDNA3.1 ATF4 WT-5′UTR-Luciferase reporter	This study	N/A
pcDNA3.1 ATF4 uORF2-Luciferase reporter	This study	N/A
pcDNA3.1 ATF4 A225G-Luciferase reporter	This study	N/A
pcDNA3.1 ATF4 A225C-Luciferase reporter	This study	N/A
pcDNA3.1 ATF4 A225T-Luciferase reporter	This study	N/A
Software and Algorithms		
Bowtie	N/A	http://bowtie-bio.sourceforge.net/index.shtml
Cutadapt	N/A	http://cutadapt.readthedocs.io/en/stable/index.html
MEME	N/A	http://meme-suite.org
Perl	Perl	https://www.perl.org
R	The R project	https://www.r-project.org

CONTACT FOR REAGENT AND RESOURCE SHARING

Further information and requests for resources and reagents should be directed to and will be fulfilled by the Lead Contact, Shu-Bing Qian (sq38@cornell.edu).

EXPERIMENTAL MODEL AND SUBJECT DETAILS

Cell lines and reagents

MEF and HEK293 cells were maintained in Dulbecco's Modified Eagle's Medium (DMEM) with 10% fetal bovine serum (FBS). Antibodies used in the immunoblotting are listed below: anti-ATF4 (Santa cruz sc-200), anti-β-actin (Sigma A5441), anti-ALKBH5 (Proteintech 16837-1-AP), anti-FTO (Phosphosolutions 597-Fto), anti-METTL3 (Proteintech 15073-1-AP), anti-METTL14 (Sigma HPA038002), anti-phosphorylated eIF2α (Cell signaling 3398P), anti- eIF2α (Cell signaling 5324), anti-RPL4 (Proteintech 11302-1-AP), anti-RPS6 (Cell signaling 2217), anti-m^6A (Millipore ABE572) and anti-m^6A (Synaptic Systems 202 003).

FTO transgenic mice

Conditional overexpression of *Fto* was achieved by transfecting Bruce4 ES cells with a vector containing *Fto* cDNA fused to a myc-tag, a 5′ loxP-flanked NeoR stop cassette and a 3′ FRT-flanked IRES eGFP. Successful targeting in ES cells was assessed by Southern blot analysis and positive clones were subsequently injected into blastocysts. High-grade chimeric mice were bred for germline transmission of the transgene. The starvation procedure was approved by the University Committee on Use and Care of Animals at the Cornell University.

METHOD DETAILS

Plasmid constructions

The pGL3 TK-ATF4 WT-5′-leader-Luciferase reporter and pGL3 TK-ATF4 uORF2 deletion-Luciferase reporter was kindly provided by Dr. Ronald C. Wek. The luciferase reporters containing ATF4 5′UTR were subcloned into pcDNA3.1 (Invitrogen) using Hind III and Xba I sites. ATF4 A225G-Luciferase reporter was generated from ATF4 WT-5′-leader-Luciferase reporter using the QuikChange II XL Site-Directed Mutagenesis Kit (Agilent Technologies).

Lentiviral shRNAs

shRNA targeting sequences are listed below. ALKBH5 (mouse): 5′- GCCTCAGGACATTAA GGAACG-3′; FTO (mouse): 5′-GCTGA GGCAGTTCTGGTTTCA-3′; METTL3 (mouse): 5′-GCTACAGGATGACGGCTTTCT-3′; METTL14 (mouse): 5′- GGATCAAAGGAAC CGTG AAGC-3′; Scramble control sequence: 5′-AACAGTCGCGTTTGCGACTGG-3′. All the shRNA targeting sequences were cloned into DECIPHER pRSI9-U6-(sh)-UbiC-TagRFP-2A-Puro (Cellecta, CA). Lentiviral particles were packaged using Lenti-X 293T cells (Clontech). Virus-containing supernatants were collected at 48 hr after transfection and filtered to eliminate cells. MEF cells were infected by the lentivirus for 48 hr before selection by 1 μg/ml puromycin.

Amino acid starvation treatment

Amino acid starvation treatment was carried out by incubating cells in HBSS buffer (Lonza) with 10% dialyzed FBS (Sigma Aldrich). Samples were collected at indicated time points.

SILAC

MEF cells cultured in 'heavy' or 'light' medium for 5 passages before 'heavy' isotope labeled cells were treated with amino acid starvation for 2 hr. Both cells were lysed in ice in polysome buffer (10 mM HEPES, pH 7.4, 100 mM KCl, 5 mM $MgCl_2$ and 100 μg/ml cycloheximide) with 1% Triton X-100 and protease inhibitor, followed by centrifugation. Equal concentration of supernatants were pooled and incubated with 15 μg/ml yeast tRNA (Invitrogen), 20U/μl SUPERase_In (Invitrogen) and 50μl equilibrated affigel-heparin beads (Biorad) for 10min at 4°C. Beads were spun down and supernatant was pre-cleared with 100μl Dynabeads M-280 Streptavidin beads (Fisher) for 1hr. The pre-cleared supernatant supplemented with 10 μg of a biotinylated oligo targeting the 3′UTR of human ATF4 (IDT, 5′>Biotin TEG GT ACA AGC ACA AAG CAC CTG ACT < 3′). The incubation was carried out for 1h at 4°C after which 50 μL of equilibrated Streptavidin beads was added and incubated for additional 2 hours at 4°C. Beads were washed and eluted by boiling in Laemmli buffer. The protein content in the eluted material was on an SDS-PAGE gel prior to band excision and in gel trypsin digestion. The resultant peptide mixtures were pressure-loaded onto a C18 reverse-phase capillary column and analyzed by online nanoflow LC-MS/MS on an Agilent 1200 quaternary HPLC system (Agilent) connected to an LTQ-Orbitrap mass spectrometer (Thermo Fisher Scientific) using a 2-h gradient. MS data were searched with ProLuCID on IP2 (Integrated Proteomics Applications) against human UniProt database, and filtered using DTASelect2 with a 5 ppm Δ mass cutoff of the peptide masses and a false-positive rate below 1%.

Immunoblotting

Cells were lysed on ice in TBS buffer (50 mM Tris, pH7.5, 150 mM NaCl, 1 mM EDTA) containing 1% Triton X-100, 2 U/ml DNase and protease inhibitor cocktail tablet. The lysates were incubated on ice for 30 min, followed heating for 10 min in SDS-PAGE sample buffer (50 mM Tris (pH6.8), 100 mM dithiothreitol, 2% SDS, 0.1% bromophenol blue, 10% glycerol). Proteins were separated on SDS-PAGE and transferred to PVDF membranes (Fisher). Membranes were blocked in TBS containing 5% non-fat milk and 0.1% Tween-20 for 1 hr, followed by incubation with primary antibodies overnight at 4°C. After incubation with horseradish peroxidase-coupled secondary antibodies at room temperature for 1 hr, immunoblots were visualized using enhanced chemiluminescence (ECL-Plus, GE Healthcare).

Real-time quantitative PCR

Total RNA was isolated by TRIzol reagent (Invitrogen) and used for reverse transcription assay via High Capacity cDNA Reverse Transcription Kit (Invitrogen). Real-time PCR analysis was conducted using Power SYBR Green PCR Master Mix (Applied Biosystems) and carried on a LightCycler 480 Real-Time PCR System (Roche Applied Science). Primers for amplifying each target are listed below:

- ATF4-Fwd: 5′- CTTGATGTCCCCCTTCGACC −3′;
- ATF4-Rev: 5′- CTTGTCGCTGGAGAACCCAT −3′.
- GAPDH-Fwd: 5′- CAAGGAGTAAGAAACCCTGGAC −3′;
- GAPDH-Rev: 5′- GGATGGAAATTGTGAGGGAGAT −3′.

m^6A dot blot

mRNA was purified from total RNA using Dynabeads Oligo(dT)25 (Thermo Fisher). Equal amounts of mRNA were spotted to a nylon membrane (Fisher), followed by UV crosslinking at UV 254 nm, 0.12 J/cm^2. After blocking in PBST containing 5% non-fat milk and 0.1% Tween-20 for 1 hr, the membrane was incubated with 1:1000 diluted anti-m^6A antibody overnight at 4°C. The membrane was incubated with HRP-conjugated anti-rabbit IgG (1:5000 dilution) for 1 hr and visualized by using enhanced chemiluminescence (ECLPlus, GE Healthcare).

Dual-luciferase assay

Firefly Luciferase reporters were co-transfected with a Renilla reporter plasmid into MEF cells or knockdown cells for 4 hr. Transfected cells were treated with amino acid starvation for 6 hr before collection. Firefly and Renilla luciferase activities were measured using Dual-Luciferase Reporter Assay System (Promega). Relative values of firefly luciferase activities were normalized to Renilla luciferase control. The relative values of firefly luciferase were shown as the average of three biological replicates.

Toeprinting

The ribosome binding reaction mixtures were prepared on ice in a total volume of 6 μl containing 50% Nuclease-treated rabbit reticulocyte lysate (Promega), 20 pmol of primer (5′- 6-FAM-AATTGTTCCAGGAACCAG-3′), 20 μM amino acid mixture minus methionine, 20 μM amino acid mixture minus leucine,0.4U/μL RNaseOUT (Invitrogen) and 50 mM Tris-HCl, pH 7.5. Reactions were added with or without 1 mg/mL CHX and incubated at 37°C for 5 min. Then the reaction mixtures were added with 0.5 μg of mRNA, followed by incubating at 30°C for 20min to allow the translation machinery to assemble. The reverse transcriptase reaction was performed in a total volume of 20 μl containing entire ribosome binding reaction, 1x Superscript III reverse transcriptase buffer, 5 mM DTT, 1 mg/ml cycloheximide, 500 μM of each of four dNTPs, 1.5U/μL RNaseOUT, 5U/μL Superscript III reverse transcriptase and incubated at 25°C for 10 min. Reactions were terminated by extracting with phenol:chloroform followed by ethanol precipitation. Primer extension products were resuspended in 10 μL of Hi-Di formamide. A 2 μL aliquot was run with 0.2 μL GeneScan 500 LIZ dye Size Standard (Fisher) on an ABI 3730xl instrument. Data were analyzed by GeneMapper software (Life Technologies).

Tth-mediated m^{6}A site-specific detection

For site-specific detection of m^{6}A, DNA primer (5′- TGCTTAACTCGAAGGTATCTTTG −3′) was first 5′ labeled with ^{32}P using T4 polynucleotide kinase (Invitrogen) and [γ-^{32}P] ATP (Perkin Elmer) and purified by ethanol precipitation. The Poly(A)$^+$ RNA was prepared using Dynabeads Oligo (dT) (Thermo Fisher Scientific) from MEF cells under normal or amino acid starvation condition. 10 μg mRNA was directly diluted in 450 μL immunoprecipitation buffer (50 mM Tris, pH 7.4, 100 mM NaCl, 0.05% NP-40) and incubated with 2.5 μg m^{6}A antibody at 4°C for 3 h, rotating head over tail. The solution was then cross-linked twice with 0.15 J cm^{-2} UV light (254 nm) in a Stratalinker (Agilent). After cross-linking, the reverse transcription was conducted with indicated ^{32}P-labeled primer and *Tth* enzyme as previous described. Generally, 10 μg m^{6}A-crosslinked mRNA was prepared in a total volume of 6 μL with *Tth* buffer (Promega) and 1 μL radiolabeled primer. The mixture was heated at 95°C for 10 min and cooled slowly to room temperature. The annealing solution were combined with 5 U of *Tth* enzyme, 1 mM $MnCl_2$ and heated at 55°C for 3 min. After adding the dTTP solution (final dTTP concentration: 100 μM), the reactions were heated for 10 minutes at 55°C. Reaction products were resolved on a 20% denaturing polyacrylamide gel and detected by autoradiography overnight.

Polysome profiling analysis

Sucrose solutions were prepared in polysome buffer (10 mM HEPES, pH 7.4, 100 mM KCl, 5 mM $MgCl_2$ and 100 μg/ml cycloheximide). A 15%- 45% (w/v) Sucrose density gradient was freshly prepared in a SW41 ultracentrifuge tube (Backman) using a Gradient Master (BioComp Instruments). Cells were lysed in polysome lysis buffer (polysome buffer and 2% Triton X-100) and cell debris were removed by centrifugation at 14,000 rpm for 10 min at 4°C. 500 μL of supernatant was loaded onto sucrose gradients followed by centrifugation for 2 h 30 min at 38,000 rpm 4°C in a SW41 rotor. Separated samples were fractionated at 0.75 ml/min through an automated fractionation system (Isco) that continually monitors OD254 values. An aliquot of ribosome fraction were used to extract total RNA using Trizol LS reagent (Invitrogen) for Ribo-seq.

RNA-seq and m^{6}A–seq

Total RNA was first isolated using Trizol reagent followed by fragmentation using freshly prepared RNA fragmentation buffer (10 mM Tris-HCl, pH 7.0, 10 mM $ZnCl_2$). 5 μg fragmented RNA was saved for RNA-seq as input control. For m^{6}A-seq, 400 μg fragmented RNA was incubated with 10 μg anti-m^{6}A antibody (Millipore ABE572) and 2.5 μg anti-m^{6}A antibody Synaptic Systems 200 203) in 1 × IP buffer (10 mM Tris-HCl, pH 7.4, 150 mM NaCl, and 0.1% Igepal CA-630) for 2 hr at 4°C. The m^{6}A-IP mixture was then incubated with Protein A/G beads for additional 2 hr at 4°C on a rotating wheel. After washing 3 times with IP buffer, bound RNA was eluted using 100 μL elution buffer (6.7 mM N^6-Methyladenosine 5′-monophosphate sodium salt in 1 × IP buffer), followed by ethanol precipitation. Precipitated RNA was used for cDNA library construction and high-throughput sequencing described below.

QTI-seq and Ribo-seq

For QTI-seq, cells were collected in 400 μL of ice-cold polysome buffer containing 5 μM LTM. Samples were transferred to a 2 mL Eppendorf tube containing Lysing Matrix-D and cells were lysed by vortexing 20 s for six times with a 40 s interval on ice. After removing the debris by centrifugation for 10 min at 13,000 × g at 4°C, supernatant were transferred to a new Eppendorf tube and supplemented with 10 mM creatine phosphate, 0.1 mM spermidine, 40 μg/mL creatine phosphokinase, 0.8 mM ATP, 20 μM ATA and 25 μM of puromycin. The mixtures were incubated at 35°C for 15 min. For both QTI-seq and Ribo-seq, ribosome fractions separated by sucrose gradient sedimentation were pooled and digested with *E. coli* RNase I (Ambion, 750 U per 100 A260 units) by

incubation at 4°C for 1 h. SUPERase inhibitor (50 U per 100 U RNase I) was then added into the reaction mixture to stop the digestion. Total RNA was extracted using TRIzol reagent. Purified RNA was used for cDNA library construction and high-throughput sequencing described below.

cDNA library construction

Fragmented RNA input or m^{6}A-IP elutes were dephosphorylated for 1 hr at 37°C in 15 μL reaction (1 × T4 polynucleotide kinase buffer, 10 U SUPERase_In and 20 U T4 polynucleotide kinase). The products were separated on a 15% polyacrylamide TBE-urea gel (Invitrogen) and visualized using SYBR Gold (Invitrogen). Selected regions of the gel corresponding to 40-60 nt (for RNA-seq and m6A-seq) or 25-35 nt (for Ribo-seq and QTI-seq) were excised. The gel slices were disrupted by using centrifugation through the holes at the bottom of the tube. RNA fragments were dissolved by soaking overnight in 400 μL gel elution buffer (300 mM NaOAc, pH 5.5, 1 mM EDTA, 0.1 U/ml SUPERase_In). The gel debris was removed using a Spin-X column (Corning), followed by ethanol precipitation. Purified RNA fragments were re-suspended in nuclease-free water. Poly-(A) tailing reaction was carried out for 45 min at 37°C (1 × poly-(A) polymerase buffer, 1 mM ATP, 0.75 U/μl SUPERase_ In and 3 U *E. coli* poly-(A) polymerase).

For reverse transcription, the following oligos containing barcodes were used:

MCA02, 5′-pCAGATCGTCGGACTGTAGAACTCTØCAAGCAGAAGACGGCATACGATT TTTTTTTTTTTTTTTTVN-3′;

LGT03, 5′-pGTGATCGTCGGACTGTAGAACTCTØCAAGCAGAAGACGGCATACGATTT TTTTTTTTTTTTTTTVN-3′;

YAG04, 5′-pAGGATCGTCGGACTGTAGAACTCTØCAAGCAGAAGACGGCATACGATT TTTTTTTTTTTTTTTTVN-3′;

HTC05, 5′-pTCGATCGTCGGACTGTAGAACTCTØCAAGCAGAAGACGGCATACGATT TTTTTTTTTTTTTTTTVN-3′, where Ø represents an abasic residue.

In brief, the tailed-RNA sample was mixed with 0.5 mM dNTP and 2.5 mM synthesized primer and incubated at 65°C for 5 min, followed by incubation on ice for 5 min. The reaction mix was then added with 1 X SuperScript III buffer, 10 mM DTT, 40 U RNaseOUT and 200 U SuperScript III and incubated at 50°C for 50 min. Reverse transcription products were separated on a 10% polyacrylamide TBE-urea gel and the corresponding region was excised as described earlier. The cDNA was recovered by using DNA gel elution buffer (300 mM NaCl, 1 mM EDTA). First-strand cDNA was circularized in 20 μL of reaction containing 1 × CircLigase buffer, 50 μM ATP, 2.5 mM $MnCl_2$ and 100 U CircLigase (Epicenter). Circularization was performed at 60°C for 1 h, and the reaction was heat inactivated at 80°C for 10 min. rRNA depletion were performed before templates amplification.

Deep sequencing

Single-stranded template was amplified by PCR by using the Phusion High-Fidelity enzyme (NEB) according to the manufacturer's instructions. The oligonucleotide primers qNTI200 (5′-CAAGCAGAAGACGGCATA-3′) and qNTI201 (5′-AATGATACGGCGACCACC GAGATC TACACGTTCAGAGTTCTACAGTCCGACG-3′) were used to create DNA suitable for sequencing, i.e., DNA with Illumina cluster generation sequences on each end and a sequencing primer binding site. The PCR contains 1 × HF buffer, 0.2 mM dNTP, 0.5 μM oligonucleotide primers, and 0.5 U Phusion polymerase. PCR was carried out with an initial 30 s denaturation at 98°C, followed by 12 cycles of 10 s denaturation at 98°C, 20 s annealing at 60°C, and 10 s extension at 72°C. PCR products were separated on a nondenaturing 8% polyacrylamide TBE gel as described earlier. Expected DNA at 120 bp (for Ribo-seq), or 140 bp (for RNA-seq and m^{6}A-seq) was excised and recovered as described earlier. After quantification by Agilent BioAnalyzer DNA 1000 assay, equal amount of barcoded samples were pooled into one sample. Approximately 3–5 pM mixed DNA samples were used for cluster generation followed by deep sequencing by using sequencing primer 5′-CGACAGGTTCAGAGTTCTA CAGTCCGACGAT C-3′ (Illumina HiSeq).

QUANTIFICATION AND STATISTICAL ANALYSIS

m^{6}A-Seq coverage analysis

m^{6}A-Seq and input RNA-Seq reads (20nt – 40nt) were aligned to NCBI RefSeq mRNA sequences and UCSC genome sequences (hg19 for human and mm10 for mouse) using Tophat (–bowtie1–no-novel-juncs -G) as described previously (Trapnell et al., 2009). All the full-length mapped reads were used to generate m^{6}A-Seq coverage profile for individual genes. To compare metagene m^{6}A profiles between control and starvation samples, the raw coverage values were first internally normalized by the mean coverage of each individual gene (for genes with multiple mRNA isoforms, the longest isoform was selected). The genes with maximal coverage value less than 15 were excluded for further consideration. The normalized m^{6}A-Seq profiles of individual gene were next subtracted by corresponding RNA-Seq profile to generate an adjusted m^{6}A-Seq profile. The metagene profile used for between-sample comparison (control versus amino acid starvation) was finally derived by averaging all the adjusted profiles of individual genes.

Ribosome profiling analysis

The Ribo-Seq and QTI-Seq data were analyzed using the same procedures as described previously (Gao et al., 2015). In brief, the p-site position (13th position) of RPF in both Ribo-Seq and QTI-Seq was extracted. The ribosome occupancy of transcripts was calculated as CDS reads per kilobase per million mappable reads (CDS RPKM). The TIS was predicted using a negative binomial model and TIS signal was normalized by upper quartile (UQ) value of all predicted TIS sites. The UQ normalized TIS signal was further normalized by the mRNA expression level (FPKM) which was estimated using Cufflinks (Trapnell et al., 2010).

Heatmap of aTIS density change and local m^{6}A level change

Genes whose 5′ UTR are less than 20nt were first excluded for the downstream analysis to ensure sufficient context for uTIS biogenesis. Genes whose total reads around aTIS (−2nt, +3nt) in the QTI-Seq were less than 10 were also disregarded. Moreover, genes whose maximal coverage around aTIS (−20nt, +60nt) in the m^{6}A-Seq were less than 15 and less than one fifth of the global maximal coverage (the whole mRNA) were also excluded. aTIS density was calculated as the ratio of average QTI-Seq density in a 5nt window (−2nt, +3nt) of aTIS to that in the remaining region of CDS.

The combined TIS datasets as predicted in the control and starvation samples were used to classify genes with regard to uTIS. Specifically, the gene with both aTIS and uTIS were defined as uTIS (Y) group. On the other hand, the genes without uTIS while embracing aTIS were defined as uTIS (N) group. A revised local Peak-Over-Median value is calculated as the ratio of the peak m^{6}A coverage of a 80nt window (−20nt, 60nt) surrounding aTIS to the sum of median coverage of whole transcript and a pseudo-number 0.5 which is used to account for sparse m^{6}A-Seq reads across the gene.

$$\text{local POM} = \frac{\text{Peak Coverage}_{\text{local region}}}{\text{Median Coverage}_{\text{full transcript}} + 0.5}$$

The fold change of local POM values between control and amino-acid starvation samples was used to evaluate the change of m^{6}A signal in the flanking region of aTIS. Hierarchical clustering (agglomeration method: Ward) was performed on aTIS density change and local m^{6}A level change for both uTIS (Y) and uTIS(N) gene groups.

Impact of 5′ UTR m^{6}A signal on ribosome occupancy

Fold change of local POM values (control versus starvation) of the second half of the 5′ UTR was calculated to reflect m^{6}A signal change in a region immediately upstream of the translation start site. Two groups of genes (1.5 fold increase and decrease in POM values) were compiled for ribosome occupancy comparison over the main CDS.

PAR-CLIP analysis

The PAR-CLIP data for ALKBH5 and METTL3 in HEK293T were retrieved from NCBI GEO (GEO: GSE38201 and GSE50580) (Baltz et al., 2012; Ping et al., 2014). Adaptor-trimmed reads with read length no less than 15 nt were mapped to human transcriptome. Only the uniquely mapped reads with no more than two mismatches were used. A method similar to PARalyzer (Corcoran et al., 2011) was employed to identify ALKBH5 and METTL3 binding sites. In brief, reads with at least one overlapping nucleotide were grouped together to form read cluster. For each cluster that contains at least 15 reads and 5 T to C mutations, a Gauss kernel density-based classifier was used to find the binding sites (see Corcoran et al., 2011 for more details).

DATA AND SOFTWARE AVAILABILITY

Statistical analysis was mainly done using GraphPad Prism and SigmaPlot (Systat Software). Unless otherwise noted, some analytical procedures were completed using custom Perl scripts. These scripts are available upon request. The accession number for the Ribo-seq and RNA-seq reported in this paper is GEO: GSE102659. Original images have been deposited to Mendeley Data and are available at https://doi.org/10.17632/p4kwsdgkck.2.